PERFORMANCE OF HETEROSIS ELEMENT FOR BENDING OF SKEW RHOMBIC PLATES

T. S. Butalia, T. Kant and V. D. Dixit

Department of Civil Engineering, Indian Institute of Technology, Powai, Bombay 400 076, India

Abstract—A critical analysis of parallelogram-shaped plates under bending using a Mindlin nine-node Heterosis element is carried out. The performance of this quadratic quadrilateral element is evaluated on isotropic rhombic skew plates up to large skew angles with different support conditions and under uniformly distributed as well as point loads. The suitability and limitations of the element for each case are clearly brought out. The numerical results of the present formulation are compared with the available data in the literature. Morley's acute skew plate involving singularity is studied in detail. Oblique boundary transformation required for all the sides simply supported boundary condition is discussed. In addition, numerical results for transverse shear forces are presented for the first time in the literature, for future reference.

INTRODUCTION

Skew plates are often used in modern structures in spite of the mathematical difficulties involved in their study. Swept wings of aeroplanes can be idealized by introducing substitute structures in the form of skew plates. Complex alignment problems in bridge design are often solved by use of skew plates due to functional, aesthetic or structural requirements. Various other applications of skew plates can be found in ship hulls, as well as parallelogram slabs in buildings.

The rigorous formulation and solution of the governing differential equation is extremely tedious due to the use of a non-orthogonal coordinate system. Analytical solution procedure requires use of a series in one form or another [1–21]. Trignometric series [1, 2], power series [1, 10, 14–16, 18], polynomial series [3, 4, 9, 13], complex series [5], biharmonic eigen-functions [6, 7] and Fourier series [8, 11, 12, 17, 19, 20] have been employed in the past for the analysis of skew plates. Recently, GangaRao and Chaudhary [21] presented a plate bending solution for skew plates using a combination of trignometric and polynomial functions with un-determined coefficients. In spite of extensive research done in the area of skew plate bending, researchers are still looking for a suitable choice for trial solution functions that could lead to more accurate and economical solutions [21]. Morley [22] presents a good overview of the analytical series solution.

Finite difference techniques have also been favourably employed [22–29] for the analysis of skew plates but have limited accuracy even for reasonably small skew angles.

The Finite Element Method has been extensively employed for small deflection analysis of thin parallelogram-shaped plates. The displacement based Kirchhoff plate bending elements [30–46], which neglect the transverse shear deformation effects, have been used for the analysis of skew plates. These thin plate elements reqire C^1 continuity of the displacement field as the variational theorem for these contains derivatives of the kinematic variables up to the second order. Reissner [47] and Mindlin [48] were the first to provide first order shear deformable theories based on the thin plate assumptions for variation of stresses and displacements through the thickness of the plate. Both these theories give rise to a sixth order partial differential system of equilibrium equations and permit satisfaction of three boundary conditions on each edge. This Reissner–Mindlin theory requires only C^0 continuity on the approximations of kinematic variables in the variational statement. Moreover, low order interpolation functions can be employed while numerical simplifications may be introduced at the element level. This theory allows adequate modelling of classical thin plates as well as moderately thick, sandwich and composite plates. The displacement based Mindlin elements [49–65] have exhibited good results for the analysis of skew plates. Akay [66] employed first and second order mixed plate bending elements for analysis. The Hybrid Stress Model [67] based on Kirchhoff theory [29] as well as Discrete Kirchhoff theory [67] has been usefully employed for analysis. Hybrid Trefftz's element [68, 69] and Lyon's modified element [70] also exhibit good results. Anisotropic skew plates [43, 51, 56] as well as skew laminated plates [49, 50] have also been studied.

In addition, various other techniques have also been used for the analysis of skew plates. Variational solution [13, 15, 22, 71–74], electrical analogy [75, 76], point matching [77, 78], conformal mapping [79, 80], equivalent grid method [81], finite strip method [82–85]

and experimental investigations [18, 24, 25, 32, 86–89] have been used. Large deflection analysis of skew plates [85, 90–92] has also been carried out.

The 'Heterosis' element is generally believed to be a safe and robust element [93, 94] and possesses numerous advantages over other elements. Therefore, it was thought appropriate to employ this element for the analysis of skew plates.

REISSNER/MINDLIN PLATE THEORY

The main assumptions in the development of this theory are as follows. (a) Displacements are small compared to plate thickness. (b) The stress σ_z normal to the midsurface is negligible. (c) The strain ϵ_z normal to the middle surface is zero. (d) Normals to the midsurface before deformation remain straight but not necessarily normal to the middle surface after deformation.

The theory is based on the kinematic displacement model (Fig. 1),

$$u(x, y, z) = z \cdot \theta_x(x, y)$$

$$v(x, y, z) = z \cdot \theta_y(x, y)$$

$$w(x, y, z) = w_0(x, y) \tag{1}$$

where u, v, and w define the displacement components in the directions x, y and z respectively. Both x and y coordinates lie in the reference plane of the plate which is assumed to be unstrained. The terms θ_x and θ_y are the usual average rotations of the normals to the reference plane along the x and y directions respectively, while w_0 defines the lateral displacement at the reference surface. Thus, the displacement vector of the reference plane is defined as

$$\delta = [w_0, \theta_x, \theta_y]^t. \tag{2}$$

The strain–displacement relations are expressed as follows:

$$\epsilon_x = \frac{\partial u}{\partial x} = z \cdot \frac{\partial \theta_x}{\partial x} = z \cdot \kappa_x$$

$$\epsilon_y = \frac{\partial v}{\partial x} = z \cdot \frac{\partial \theta_y}{\partial y} = z \cdot \kappa_y$$
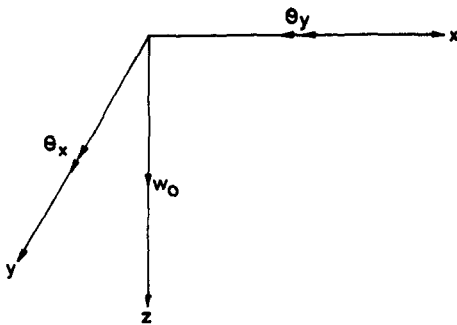
Fig. 1. Positive set of displacement components.

$$\gamma_{xy} = \frac{\partial u}{\partial y} + \frac{\partial v}{\partial x} = z \cdot \left[\frac{\partial \theta_x}{\partial y} + \frac{\partial \theta_y}{\partial x} \right] = z \cdot \kappa_{xy}$$

$$\gamma_{xz} = \frac{\partial u}{\partial z} + \frac{\partial w}{\partial x} = \theta_x + \frac{\partial w_0}{\partial x} = \Phi_x$$

$$\gamma_{yz} = \frac{\partial v}{\partial z} + \frac{\partial w}{\partial y} = \theta_y + \frac{\partial w_0}{\partial y} = \Phi_y. \tag{3}$$

If we define

$$\epsilon_b^t = [\epsilon_x, \epsilon_y, \gamma_{xy}] = z \cdot [\kappa_x, \kappa_y, \kappa_{xy}]$$

$$\epsilon_s^t = [\gamma_{xz}, \gamma_{yz}] = [\phi_x, \phi_y]$$

$$\epsilon^t = [\epsilon_b^t, \epsilon_s^t] \tag{4}$$

and

$$\sigma_b^t = [\sigma_x, \sigma_y, \tau_{xy}]$$

$$\sigma_s^t = [\tau_{xz}, \tau_{yz}]$$

$$\sigma^t = [\sigma_b^t, \sigma_s^t], \tag{5}$$

then the 3D stress–strain relations can be written in a compact form as follows:

$$\sigma_b = E_b \cdot \epsilon_b$$

$$\sigma_s = E_s \cdot \epsilon_s$$

$$\sigma = E \cdot \epsilon, \tag{6}$$

where

$$E_b = \begin{bmatrix} E_{11} & E_{12} & 0 \\ E_{12} & E_{22} & 0 \\ 0 & 0 & E_{33} \end{bmatrix}$$

$$E_s = \begin{bmatrix} E_{s1} & 0 \\ 0 & E_{s2} \end{bmatrix}. \tag{7}$$

For an isotropic material, the elastic constants are

$$E_{11} = E_{22} = \frac{E}{(1 - v^2)}$$

$$E_{12} = v \cdot E_{11}$$

$$E_{33} = \frac{1 - v}{2} E_{11} = \frac{E}{2(1 + v)} = G$$

$$E_{s1} = E_{s2} = G. \tag{8}$$

The total potential energy expression is written as

$$\Pi = U - W$$

$$= \frac{1}{2} \int_v \epsilon^t \cdot \sigma \cdot dv - \int_v u^t \cdot b \cdot dv, \tag{9}$$

where

$u^t = [u, v, w]$ is the vector of displacement components of a point in the plate space

$\mathbf{b}$ = vector of body forces

v = domain of interest.

Total strain energy U can be split into two components for bending (U_b) and shear (U_s) as follows:

$$U = U_b + U_s$$

$$= \frac{1}{2}\int_v \epsilon_b^t \cdot \sigma_b \, dv + \frac{1}{2}\int_v \epsilon_s^t \cdot \sigma_s \, dv$$

$$= \frac{1}{2}\int_v (\sigma_x \cdot \epsilon_x + \sigma_y \cdot \epsilon_y + \tau_{xy} \cdot \gamma_{xy}) \, dv$$

$$+ \frac{1}{2}\int_v (\tau_{xz} \cdot \gamma_{xz} + \tau_{yz} \cdot \gamma_{yz}) \, dv$$

$$= \frac{1}{2}\int_v (\sigma_x \cdot z \cdot \kappa_x + \sigma_y \cdot z \cdot \kappa_y + \tau_{xy} \cdot z \cdot \kappa_{xy}) \, dA \cdot dz$$

$$+ \frac{1}{2}\int_v (\tau_{xz} \cdot \phi_x + \tau_{yz} \cdot \phi_y) \, dA \cdot dz$$

$$= \frac{1}{2}\int_A \left[\kappa_x \left(\int_z \sigma_x \cdot z \cdot dz \right) + \kappa_y \left(\int_z \sigma_y \cdot z \cdot dz \right) \right.$$

$$+ \kappa_{xy} \left(\int_z \tau_{xy} z \cdot dz \right) \bigg] dA + \frac{1}{2}\int_A \left[\phi_x \left(\int_z \tau_{xz} \cdot dz \right) \right.$$

$$+ \phi_y \left(\int_z \tau_{yz} \cdot dz \right) \bigg] dA$$

$$= \frac{1}{2}\int_v [\kappa_x \cdot M_x + \kappa_y \cdot M_y + \kappa_{xy} M_{xy}] \, dA$$

$$+ \frac{1}{2}\int_v [\phi_x \cdot Q_x + \phi_y \cdot Q_y] \, dA \tag{10}$$

in which

$$M_x = \int_z \sigma_x \cdot z \cdot dz$$

$$M_y = \int_z \sigma_y \cdot z \cdot dz$$

$$M_{xy} = \int_z \tau_{xy} \cdot z \cdot dz$$

$$Q_x = \int_z \tau_{xz} \cdot dz$$

$$Q_y = \int_z \tau_{yz} \cdot dz. \tag{11}$$

Thus we may define

$$U = \frac{1}{2}\int_A \bar{\epsilon}_b^t \cdot \bar{\sigma}_b \, dA + \frac{1}{2}\int_A \bar{\epsilon}_s^t \cdot \bar{\sigma}_s \, dA, \tag{12}$$

in which

$$\bar{\epsilon}_b^t = [\kappa_x, \kappa_y, \kappa_{xy}]$$

$$\bar{\epsilon}_s^t = [\phi_x, \phi_y]$$

$$\bar{\epsilon}^t = [\bar{\epsilon}_b^t, \bar{\epsilon}_s^t] \quad \text{generalized strain vector;} \tag{13}$$

$$\bar{\sigma}_b^t = [M_x, M_y, M_{xy}]$$

$$\bar{\sigma}_s^t = [Q_x, Q_y]$$

$$\bar{\sigma}^t = [\bar{\sigma}_b^t, \bar{\sigma}_s^t] \quad \text{generalized stress vector;} \tag{14}$$

and

$$\bar{\sigma}_b = \underline{D}_b \cdot \bar{\epsilon}_b$$

$$\bar{\sigma}_s = \underline{D}_s \cdot \bar{\epsilon}_s$$

$$\bar{\sigma} = \underline{D} \cdot \bar{\epsilon}. \tag{15}$$

Thus the 3D deformation problem is reduced to a 2D plate bending problem in which all the quantities are defined at the middle surface of the plate.

The middle surface strains are

$$\bar{\epsilon} = \left\{ \begin{matrix} \bar{\epsilon}_b \\ \bar{\epsilon}_s \end{matrix} \right\} = \begin{bmatrix} 0 & \partial/\partial x & 0 \\ 0 & 0 & \partial/\partial y \\ 0 & \partial/\partial y & \partial/\partial x \\ \partial/\partial x & 1 & 0 \\ \partial/\partial y & 0 & 1 \end{bmatrix} \left\{ \begin{matrix} w_0 \\ \theta_x \\ \theta_y \end{matrix} \right\}$$

$$= \left[\frac{\underline{L}_b}{\underline{L}_s} \right] \cdot \bar{\delta} = \underline{L} \cdot \bar{\delta}. \tag{16}$$

These can also be written separately as follows:

$$\bar{\epsilon}_b = \underline{L}_b \cdot \bar{\delta}$$

$$\bar{\epsilon}_s = \underline{L}_s \cdot \bar{\delta}, \tag{17}$$

where

$$\underline{L}_b = \begin{bmatrix} 0 & \partial/\partial x & 0 \\ 0 & 0 & \partial/\partial y \\ 0 & \partial/\partial y & \partial/\partial x \end{bmatrix}$$

and

$$\underline{L}_s = \begin{bmatrix} \partial/\partial x & 1 & 0 \\ \partial/\partial y & 0 & 1 \end{bmatrix}. \tag{18}$$

The generalized elasticity matrices $\underline{D}_b$ and $\underline{D}_s$ are expressed as

$$\underline{D}_b = \begin{bmatrix} D_{11} & D_{12} & 0 \\ D_{12} & D_{22} & 0 \\ 0 & 0 & D_{33} \end{bmatrix}$$

and

$$\underline{D}_s = \begin{bmatrix} D_{s1} & 0 \\ 0 & D_{s2} \end{bmatrix}. \tag{19}$$

For an isotropic material, the various coefficients in eqn (19) are

$$D_{11} = D_{22} = \frac{Et^3}{12(1 - v^2)}$$

$$D_{12} = v \cdot D_{11}$$

$$D_{33} = \frac{1-v}{2} D_{11} = \frac{Gt^3}{12}$$

$$D_{s1} = D_{s2} = k \cdot G \cdot t, \qquad (20)$$

where $G = E/2(1+v)$ and the shear correction factor $k = 5/6$.

Thus, the total potential energy in the generalized 2D plate bending problem is

$$\Pi = U_b + U_s - W$$

$$= \frac{1}{2} \int_A \bar{\epsilon}_b^t \cdot \bar{\sigma}_b \cdot dA + \frac{1}{2} \int_A \bar{\epsilon}_s^t \cdot \bar{\sigma}_s \cdot dA$$

$$- \int_A w_0 \cdot \bar{p}_z \cdot dA$$

$$= \frac{1}{2} \int_A \bar{\epsilon}_b^t \cdot \underline{D}_b \cdot \bar{\epsilon}_b \cdot dA + \frac{1}{2} \int_A \bar{\epsilon}_s^t \cdot \underline{D}_s \cdot \bar{\epsilon}_s \cdot dA$$

$$- \int_A \bar{\delta}^t \cdot \bar{p} \cdot dA, \qquad (21)$$

where

$$\bar{\delta}^t = [w_0, \theta_x, \theta_y]$$

$$\bar{p}^t = [\bar{p}_z, 0, 0]$$

$\bar{p}_z$ is the transverse distributed load. $\qquad (22)$

FINITE ELEMENT DISCRETIZATION

The solution of the fundamental eqns (1)–(22) presented earlier can conveniently be obtained using a finite element displacement formulation. The element properties are derived from the principle of minimum potential energy by assuming a displacement field which ensures completeness within the element and compatibility across the element boundaries.

We assume an 'NN' noded element having three degrees of freedom per node, namely w_0, θ_x and θ_y. The generalized displacement vector $\bar{\delta}$ and the nodal displacement vector $\bar{\delta}_i$ are related with the help of shape functions as

$$\bar{\delta} = \begin{Bmatrix} w_0 \\ \theta_x \\ \theta_y \end{Bmatrix} \simeq \begin{Bmatrix} \sum_{i=1}^{NN} N_i^{w_0}(x,y) \cdot w_{0i} \\ \sum_{i=1}^{NN} N_i^{\theta_x}(x,y) \cdot \theta_{xi} \\ \sum_{i=1}^{NN} N_i^{\theta_y}(x,y) \cdot \theta_{yi} \end{Bmatrix}$$

$$= \sum_{i=1}^{NN} \begin{bmatrix} N_i^{w_0} & 0 & 0 \\ 0 & N_i^{\theta_x} & 0 \\ 0 & 0 & N_i^{\theta_y} \end{bmatrix} \begin{Bmatrix} w_{0i} \\ \theta_{xi} \\ \theta_{yi} \end{Bmatrix}, \qquad (23)$$

i.e.

$$\bar{\delta} \simeq \sum_{i=1}^{NN} \underline{N}_i \cdot \bar{\delta}_i, \qquad (24)$$

where

$$\underline{N}_i = \begin{bmatrix} N_i^{w_0} & 0 & 0 \\ 0 & N_i^{\theta_x} & 0 \\ 0 & 0 & N_i^{\theta_y} \end{bmatrix}. \qquad (25)$$

If we define

$$\mathbf{d}^t = [w_{01}, \theta_{x1}, \theta_{y1} \;\vdots\; w_{02}, \theta_{x2}, \theta_{y2} \;\vdots\; \cdots \;\vdots\; w_{0i}, \theta_{xi}, \theta_{yi} \;\vdots\; \cdots \;\vdots\; w_{0NN}, \theta_{xNN}, \theta_{yNN}] \qquad (26)$$

and

$$\underline{N} = \begin{bmatrix} N_1^{w_0} & 0 & 0 & \vdots & N_2^{w_0} & 0 & 0 & \vdots & & \vdots & N_i^{w_0} & 0 & 0 & \vdots & & \vdots & N_{NN}^{w_0} & 0 & 0 \\ 0 & N_1^{\theta_x} & 0 & \vdots & 0 & N_2^{\theta_x} & 0 & \vdots & \cdots & \vdots & 0 & N_i^{\theta_x} & 0 & \vdots & \cdots & \vdots & 0 & N_{NN}^{\theta_x} & 0 \\ 0 & 0 & N_1^{\theta_y} & \vdots & 0 & 0 & N_2^{\theta_y} & \vdots & & \vdots & 0 & 0 & N_i^{\theta_y} & \vdots & & \vdots & 0 & 0 & N_{NN}^{\theta_y} \end{bmatrix} \qquad (27)$$

then

$$\bar{\delta} = \underline{N} \cdot \mathbf{d}. \qquad (28)$$

The generalized strain vectors for bending and shear are

$$\bar{\epsilon}_b = \underline{L}_b \cdot \bar{\delta} \simeq \underline{L}_b \sum_{i=1}^{NN} \underline{N}_i \cdot \bar{\delta}_i$$

$$= \sum_{i=1}^{NN} \underline{B}_{bi} \cdot \bar{\delta}_i \quad \because \quad \underline{B}_{bi} = \underline{L}_b \cdot \underline{N}_i$$

$$= \underline{B}_b \mathbf{d}$$

$$\bar{\epsilon}_s = \underline{L}_s \cdot \bar{\delta} \simeq \underline{L}_s \sum_{i=1}^{NN} \underline{N}_i \cdot \bar{\delta}_i$$

$$= \sum_{i=1}^{NN} \underline{B}_{si} \cdot \bar{\delta}_i \quad \because \quad \underline{B}_{si} = \underline{L}_s \cdot \underline{N}_i$$

$$= \underline{B}_s \mathbf{d}, \qquad (29)$$

where

$$\underline{B}_{bi} = \begin{bmatrix} 0 & \dfrac{\partial N_i^{\theta_x}}{\partial x} & 0 \\[2ex] 0 & 0 & \dfrac{\partial N_i^{\theta_y}}{\partial y} \\[2ex] 0 & \dfrac{\partial N_i^{\theta_x}}{\partial y} & \dfrac{\partial N_i^{\theta_y}}{\partial x} \end{bmatrix}$$

$$\underline{B}_{si} = \begin{bmatrix} \dfrac{\partial N_i^{w_0}}{\partial x} & N_i^{\theta_x} & 0 \\[2ex] \dfrac{\partial N_i^{w_0}}{\partial y} & 0 & N_i^{\theta_y} \end{bmatrix}. \qquad (30)$$

Thus,

$$\Pi^e \simeq \frac{1}{2} \sum_{i=1}^{NN} \sum_{j=1}^{NN} \boldsymbol{\delta}_i^t \cdot \underline{K}_{bij}^e \cdot \boldsymbol{\delta}_j$$

$$+ \frac{1}{2} \sum_{i=1}^{NN} \sum_{j=1}^{NN} \boldsymbol{\delta}_i^t \cdot \underline{K}_{sij}^e \cdot \boldsymbol{\delta}_j - \sum_{i=1}^{NN} \boldsymbol{\delta}_i^t \cdot \mathbf{f}_i^e$$

$$= \tfrac{1}{2} \mathbf{d}^t \cdot \underline{K}_b^e \cdot \mathbf{d} + \tfrac{1}{2} \mathbf{d}^t \cdot \underline{K}_s^e \cdot \mathbf{d} - \mathbf{d}^t \cdot \mathbf{f}^e, \qquad (31)$$

where the contributions to the submatrix of the element stiffness matrices linking nodes i and j are given by

$$\underline{K}_{ij}^e = \underline{K}_{bij}^e + \underline{K}_{sij}^e, \qquad (32)$$

in which

$$\underline{K}_{bij}^e = \int\int_A \underline{B}_{bi}^t \cdot \underline{D}_b \cdot \underline{B}_{bj} \cdot \mathrm{d}A$$

$$\underline{K}_{sij}^e = \int\int_A \underline{B}_{si}^t \cdot \underline{D}_s \cdot \underline{B}_{sj} \cdot \mathrm{d}A, \qquad (33)$$

and the consistent load vector for node i is given by

$$\mathbf{f}_i^e = \int\int_A \underline{N}_i^t \cdot \mathbf{b} \cdot \mathrm{d}A. \qquad (34)$$

If total number of elements is NE, the total potential energy is computed by summing the individual element's contributions such that

$$\Pi \simeq \sum_{e=1}^{NE} \Pi^e. \qquad (35)$$

The minimization of Π and Π^e leads to the system and the element equations of equilibrium respectively, as follows:

$$\underline{K} \cdot \mathbf{D} = \mathbf{f} \qquad (36)$$

$$\underline{K}^e \mathbf{d} = \mathbf{f}^e, \qquad (37)$$

in which

$$\underline{K} = \sum_{e=1}^{NE} \underline{K}^e$$

$$\mathbf{f} = \sum_{e=1}^{NE} \mathbf{f}^e, \qquad (38)$$

and $\mathbf{D}$ defines the total system degrees of freedom.

ISOPARAMETRIC REPRESENTATION

In isoparametric representation, the geometry and the displacement fields are interpolated using the same shape functions. However, while using isoparametric formulation the following interesting

points need to observed. (a) The isoparametric concept allows any arbitrary geometry to be closely approximated thereby reducing any error associated with modelling the geometry and without resorting to use of a fine mesh along the boundaries. (b) The rigid body displacement as well as constant strain criteria are satisfied. (c) Numerical integration can be carried out conveniently as a standard procedure for evaluating the integrals.

The space coordinates are expressed as

$$\begin{Bmatrix} x \\ y \end{Bmatrix} \simeq \sum_{i=1}^{NN} \begin{bmatrix} N_i & 0 \\ 0 & N_i \end{bmatrix} \begin{Bmatrix} x_i \\ y_i \end{Bmatrix}, \qquad (39)$$

where x_i and y_i are the coordinates of the node i and $N_i^{w_0} = N_i^{\theta_x} = N_i^{\theta_y} = N_i$ are shape functions in the local coordinate system $(-1 \leqslant \xi \leqslant 1, -1 \leqslant \eta \leqslant 1)$.

The Jacobian matrix of the element is defined as

$$\underline{J} = \begin{bmatrix} \partial x/\partial \xi & \partial y/\partial \xi \\ \partial x/\partial \eta & \partial y/\partial \eta \end{bmatrix} \qquad (40)$$

$$= \begin{bmatrix} \displaystyle\sum_{i=1}^{NN} \frac{\partial N_i}{\partial \xi} \cdot x_i & \displaystyle\sum_{i=1}^{NN} \frac{\partial N_i}{\partial \xi} \cdot y_i \\ \displaystyle\sum_{i=1}^{NN} \frac{\partial N_i}{\partial \eta} \cdot x_i & \displaystyle\sum_{i=1}^{NN} \frac{\partial N_i}{\partial \eta} \cdot y_i \end{bmatrix}. \qquad (41)$$

To evaluate the Cartesian shape function derivatives the chain rule of differentiation is followed, so that

$$\frac{\partial N_i}{\partial x} = \frac{\partial N_i}{\partial \xi} \cdot \frac{\partial \xi}{\partial x} + \frac{\partial N_i}{\partial \eta} \cdot \frac{\partial \eta}{\partial x}$$

$$\frac{\partial N_i}{\partial y} = \frac{\partial N_i}{\partial \xi} \cdot \frac{\partial \xi}{\partial y} + \frac{\partial N_i}{\partial \eta} \cdot \frac{\partial \eta}{\partial y} \qquad (42)$$

$$\mathrm{d}A = \mathrm{d}x \cdot \mathrm{d}y = |\underline{J}| \cdot \mathrm{d}\xi \cdot \mathrm{d}\eta. \qquad (43)$$

Thus

$$\underline{K}_{bij}^e = \int_{-1}^{+1} \int_{-1}^{+1} \underline{B}_{bi}^t \cdot \underline{D}_b \cdot \underline{B}_{bj} \cdot |\underline{J}| \cdot \mathrm{d}\xi \cdot \mathrm{d}\eta \qquad (44)$$

$$\underline{K}_{sij}^e = \int_{-1}^{+1} \int_{-1}^{+1} \underline{B}_{si}^t \cdot \underline{D}_s \cdot \underline{B}_{sj} \cdot |\underline{J}| \cdot \mathrm{d}\xi \cdot \mathrm{d}\eta \qquad (45)$$

$$\mathbf{f}_i^e = \int_{-1}^{+1} \int_{-1}^{+1} \underline{N}_i^t \cdot \mathbf{b} \cdot |\underline{J}| \cdot \mathrm{d}\xi \cdot \mathrm{d}\xi. \qquad (46)$$

THE HETEROSIS ELEMENT

The nine-node Heterosis quadrilateral element exhibits improved characteristics in comparison with the eight-node serendipity and nine-node Lagrange elements [93, 94]. In particular, the element stiffness matrix possesses correct rank and good accuracy is achieved for thin plate situations.

The element as shown in Fig. 2 has three degrees of freedom $(w_0, \theta_x, \theta_y)$ per boundary node $i = 1, 2,$

o : w_0, θ_x AND θ_y DEFINED

● : θ_x AND θ_y DEFINED

DEGREES OF FREEDOM PER ELEMENT = 26
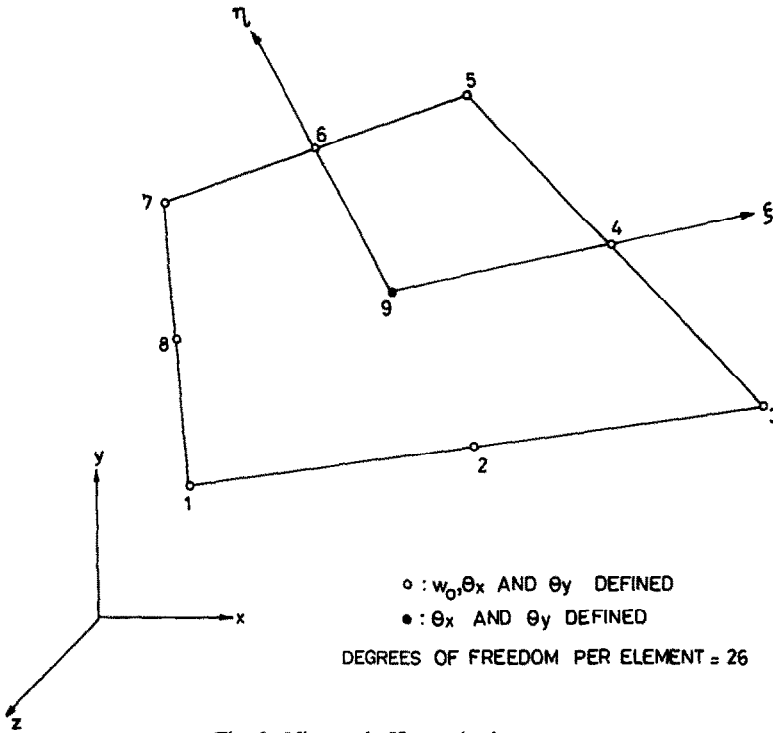
Fig. 2. Nine-node Heterosis element.

3–8 and only two degrees of freedom (θ_x, θ_y) for the central node $i = 9$. The serendipity shape functions are employed for the transverse displacement w_0, and the Lagrange shape functions for the rotations θ_x and θ_y. The selective reduced integration scheme, in which the shear energy is evaluated by a one order lower Gauss quadrature than the one required for exact integration of bending energy, has been resorted to throughout.

However, for research purposes, it is useful to implement the eight-node serendipity (S8), nine-node Lagrange (L9) as well as the present nine-node Heterosis (H9) quadrilateral elements in one code and thus a hierarchical formulation has been adopted. Thus, for a typical element e the following shape functions are adopted (Fig. 2):

for corner nodes $i = 1, 3, 5, 7$

$$N_i = \tfrac{1}{4}(1 + \xi\xi_i)(1 + \eta\eta_i)(\xi\xi_i + \eta\eta_i - 1), \quad (47)$$

for midside nodes $i = 2, 4, 6, 8$

$$N_i = \frac{\xi_i^2}{2}(1 + \xi\xi_i)(1 - \eta^2) + \frac{\eta_i^2}{2}(1 + \eta\eta_i)(1 - \xi^2). \quad (48)$$

For central node $i = 9$, the bubble function used is

$$N_i = (1 - \xi^2)(1 - \eta^2). \quad (49)$$

The hierarchical degrees of freedom at the central node $i = 9$ are viewed as the perturbations from the associated serendipity interpolants. To choose any

out of S8, L9 and H9 we can proceed as follows. (a) To obtain the S8 element, all degrees of freedom at central node $i = 9$ are constrained to zero to obtain a 24 degrees of freedom quadrilaterial element. (b) To obtain L9, all degrees of freedom at central node $i = 9$ are permitted so as to obtain a 27 degrees of freedom quadrilateral element. (c) To obtain the Heterosis element H9, the lateral displacement degree of freedom at the central node $i = 9$ is restrained to zero to generate a 26 degrees of freedom quadrilateral element.

OBLIQUE BOUNDARY TRANSFORMATION

For skew plates simply supported on two adjacent edges and even for shells, the edges of the boundary elements may not be parallel to the global axes x and y. Thus, we cannot specify the boundary conditions in terms of the global displacements w_0, θ_x and θ_y. To specify the boundary conditions at the oblique edge, we must use the local edge displacements w_0, θ_t and θ_n. θ_t and θ_n are the usual average rotations of the normals to the reference plane, tangential and normal to the oblique edge respectively. It is thus necessay to transform the element matrices corresponding to global axes (x, y, z) to local edge axes (t, n, z) along which the boundary conditions can be conveniently specified.

Considering θ_x, θ_y, θ_t and θ_n as vectors (Fig. 3)

$$\theta_x = \theta_t \cdot \cos r - \theta_n \cdot \sin r$$

$$\theta_y = \theta_t \cdot \sin r + \theta_n \cdot \cos r. \quad (50)$$
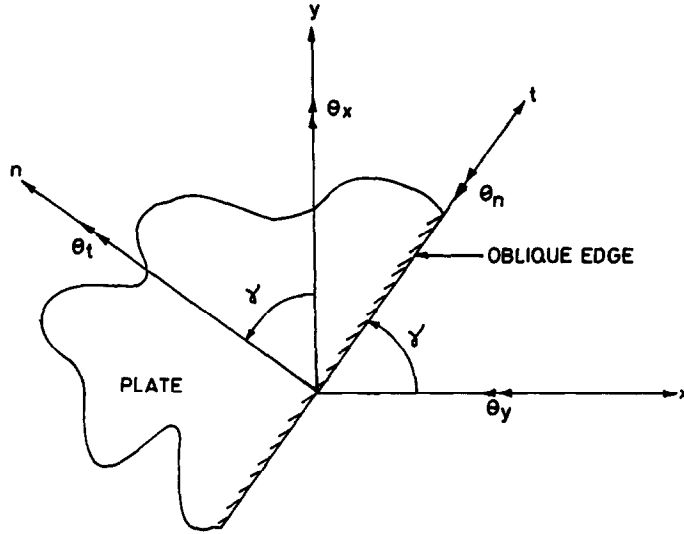
t : Axis along oblique edge
n : Axis normal to oblique edge
x, y : Global coordinate system
n,t : Local edge coordinate system

Fig. 3. Global and local edge coordinate system for oblique boundary transformation.

So, the displacement transformation for a node i on the oblique boundary is fixed as

$$\begin{Bmatrix} w_0 \\ \theta_x \\ \theta_y \end{Bmatrix} = \begin{bmatrix} 1 & 0 & 0 \\ 0 & \cos r & -\sin r \\ 0 & \sin r & \cos r \end{bmatrix} \begin{Bmatrix} w_0 \\ \theta_t \\ \theta_n \end{Bmatrix},$$ (51)

i.e.

$$\boldsymbol{\delta}_i = \underline{T}_{in} \cdot \boldsymbol{\delta}'_i,$$ (52)

where $\boldsymbol{\delta}_i$ and $\boldsymbol{\delta}'_i$ are the generalized displacement vectors in the global and local edge coordinate system respectively. The node transformation matrix for a node i on the boundary is

$$\underline{T}_{in} = \begin{bmatrix} 1 & 0 & 0 \\ 0 & \cos r & -\sin r \\ 0 & \sin r & \cos r \end{bmatrix}.$$ (53)

The above matrix is valid only for three degrees of freedom (w_0, θ_x and θ_y) per node. For higher degrees of freedom per node, a similar node transformation matrix can be found out by treating each degree of freedom as a vector. For nodes which are not on the oblique boundary, the node transformation matrix consists of all elements being zero except the principal diagonal elements, which are equal to unity. Thus, for an 'NN'-noded boundary element, the element transformation matrix is written as

$$\underline{T}_e = \begin{bmatrix} \underline{T}_{1n} & & & & & \\ & \underline{T}_{2n} & & & & \\ & & \ddots & & & \\ & & & \underline{T}_{in} & & \\ & & & & \ddots & \\ & & & & & \underline{T}_{NNn} \end{bmatrix}.$$ (54)

However, in the global system

$$\underline{K}^e \cdot \mathbf{d} = \mathbf{f}^e.$$ (55)

The vectors $\mathbf{d}$ and $\mathbf{f}^e$ undergo transformation using the same transformation matrix $\underline{T}_e$ as follows:

$$\mathbf{d} = \underline{T}_e \cdot \mathbf{d}'$$ (56)

$$\mathbf{f}^e = \underline{T}_e \cdot \mathbf{f}^{e'}.$$ (57)

So, eqn (55) becomes

$$\underline{K}^e \cdot \underline{T}_e \cdot \mathbf{d}' = \underline{T}_e \cdot \mathbf{f}^{e'}.$$ (58)

Pre-multiplying both sides by $\underline{T}_e^{-1}$

$$\underline{T}_e^{-1} \cdot \underline{K}^e \cdot \underline{T}_e \cdot \mathbf{d}' = \underline{T}_e^{-1} \cdot \underline{T}_e \cdot \mathbf{f}^{e'}$$

$$(\underline{T}_e^t \cdot \underline{K}^e \cdot \underline{T}_e) \cdot \mathbf{d}' = \underline{I} \cdot \mathbf{f}^{e'}$$

$$\because \ \underline{T}_e^{-1} = \underline{T}_e^t \quad \text{and} \quad \underline{T}_e^{-1} \cdot \underline{T}_e = \underline{I}.$$

Thus,

$$\underline{K}^{e'} \cdot \mathbf{d}' = \mathbf{f}^{e'},$$ (59)

where

$$\underline{K}^{e'} = \underline{T}_e^t \cdot \underline{K}^e \cdot \underline{T}_e.$$ (60)

In effect, for the boundary elements the first two transformations carried out are

$$\underline{K}^{e'} = \underline{T}_e^t \cdot \underline{K}^e \cdot \underline{T}_e$$

$$\mathbf{f}^{e'} = \underline{T}_e^t \cdot \mathbf{f}^e.$$ (61)
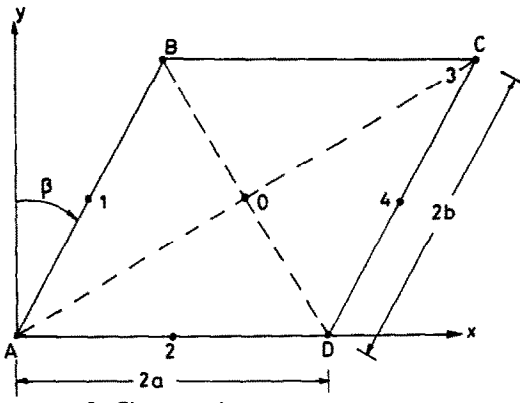
β = Skew angle
a/b = Aspect ratio(=1for rhombic plate)

Fig. 4. Skew rhombic $(a = b)$ plate.

The displacements for the nodes on the boundary are then converted from the local edge coordinate system to the global system of coordinates as per eqn (52).

NUMERICAL EXAMPLES

A computer program has been developed for numerical computation of various types of examples. All computations have been performed on the CDC CYBER 180/840 system in single precision with 14 significant digits of real rounded arithmetic accuracy (word length).

Except where specifically mentioned, the following values are adopted for analysis (Fig. 4):

$2a = 2b = 8$
t (thickness of plate) $= 0.08$
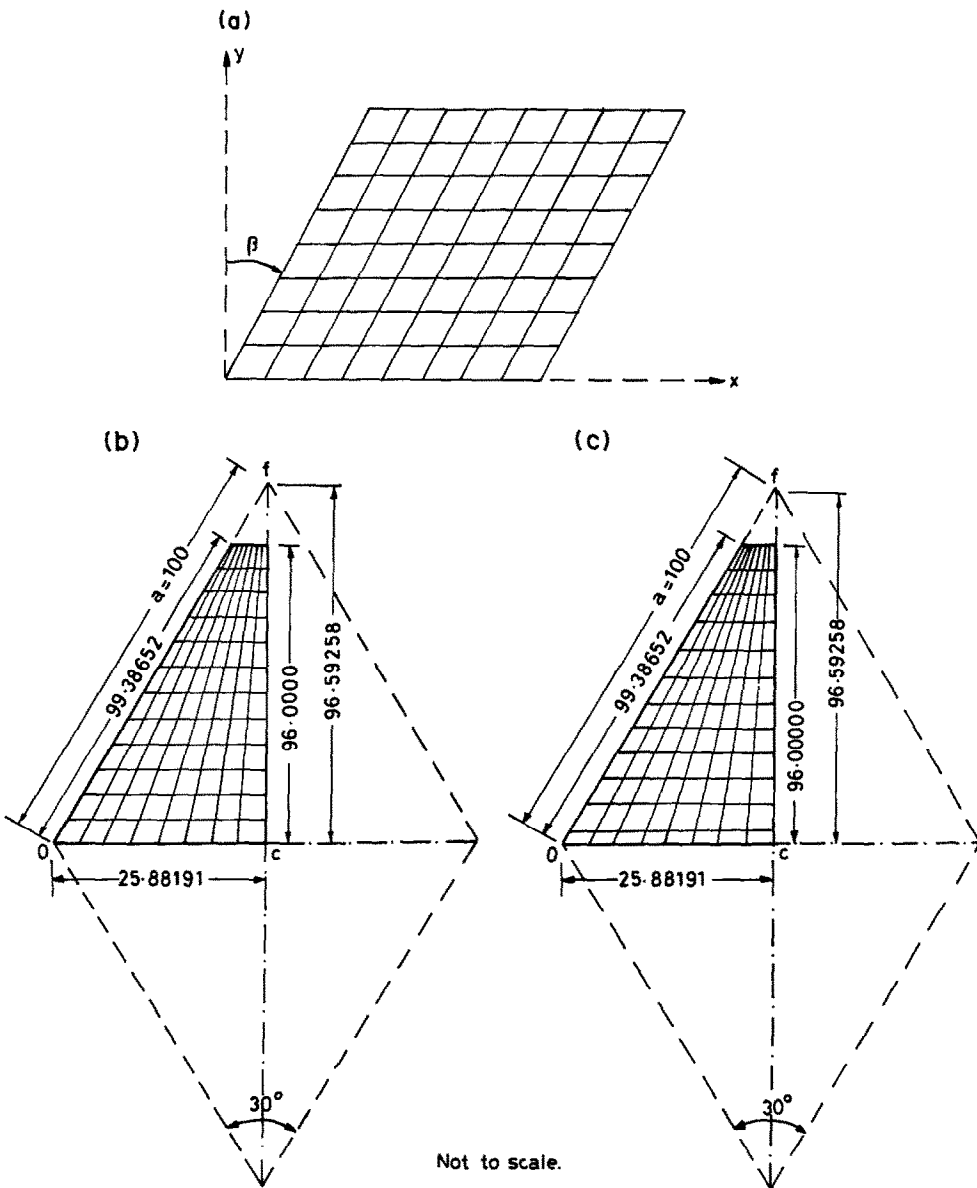
Not to scale.

Fig. 5. (a) Skew mesh (8 × 8). (b) Non-refined special mesh (8 × 12). (c) Refined special mesh (8 × 12).
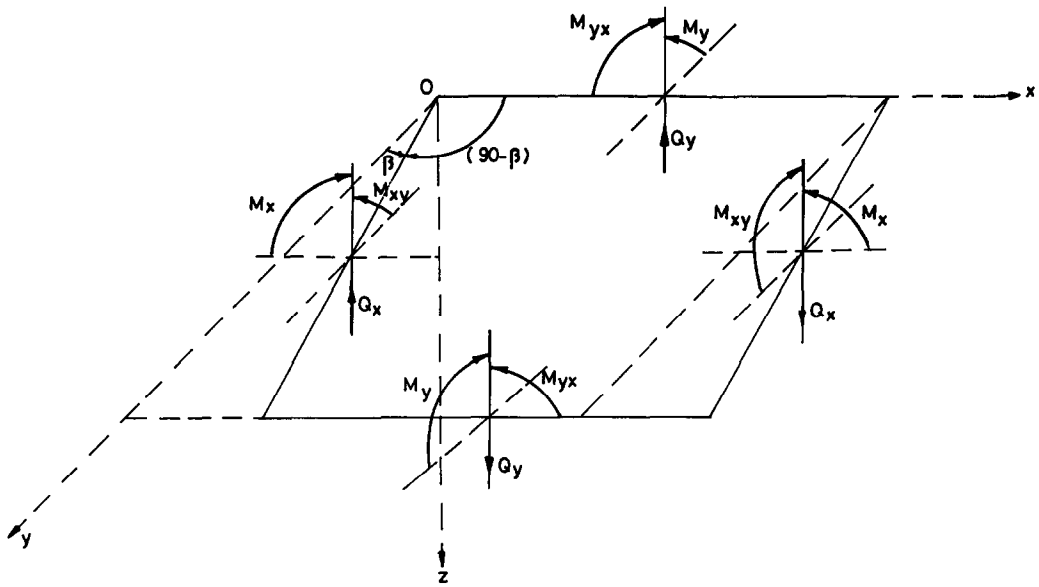
Fig. 6. Positive set of bending moment and shear forces.

E (Young's modulus of elasticity) $= 8.736 \times 10^7$
v (Poisson's ratio) $= 0.3$
D (plate rigidity) $= Et^3/12(1 - v^2) = 4096$
k (shear correction coefficient) $= 5/6$
$2a/t$ (side to thickness ratio) $= 100$
q (uniformly distributed load) $= 16$
Q (concentrated load) $= 64$.   (62)

In general an 8×8 skew mesh using a Heterosis element (H9) as shown in Fig. 5a is adopted except for convergence study and Morley's acute skew plate problem. A selective reduced integration scheme based on Gauss Legendre product rules, viz. 3×3 and 2×2, has been employed for flexural and shear contributions respectively. A bilinear extrapolation of Gauss point stresses is carried out to obtain nodal stresses. All results have been presented in non-dimensional form so that they may be applicable for a set of values other than those mentioned previously.

The boundary conditions considered in the present study are

clamped (CL): $w_0 = \theta_n = \theta_t = 0$
just supported (SS1): $w_0 = 0$
simply supported (SS2): $w_0 = \theta_t = 0$,   (63)

where θ_n and θ_t are the normal and tangential rotations of an edge respectively. The notations adopted for the stresses are shown in Fig. 6.

Example 1

Test for locking: a clamped (CL) skew plate with skew angle (β) of $45°$ subjected to uniformly distributed transverse load is considered. Central deflection results normalized with respect to Morley's [22] analytical solution are presented in

Fig. 7 for side to thickness ratio $(2a/t)$ ranging from 5 to 1000 using an 8×8 skew mesh.

Example 2

Convergence study: a clamped (CL) skew plate with large skew angle of $75°$ subjected to uniformly distributed transverse load is considered. Graphical results normalized with respect to Iyengar and Srinivasan [17] are presented in Fig. 8 using 2×2, 4×4, 6×6, and 8×8 skew mesh. From the results of Examples 1 and 2, an 8×8 skew mesh with a side to thickness ratio $(2a/t)$ equal to 100 is considered adequate for further analysis.

Example 3

Clamped skew plate: a skew plate having all edges AB, BC, CD and AD (see Fig. 4) as clamped (CL) for various skew angles (β) under uniformly distributed load as well as central concentrated load is analysed. The results in the form of maximum central deflection, maximum and minimum principal bending moment at centre as well as shear forces at points 1 and 2 (see Fig. 4) are presented in Tables 1 and 2.

For uniformly loaded plate good agreement of central deflection with that of Iyengar and Srinivasan [17] is achieved even up to a large skew angle of $75°$. Maximum principal bending moment also agrees reasonably well. Deflection profiles for various skew angles along section 'de' are shown in Fig. 9.

For central concentrated load, limited comparison for only central deflection is available up to $45°$ skew angle. Deflection profiles for various skew angles along section 'de' are shown in Fig. 10.
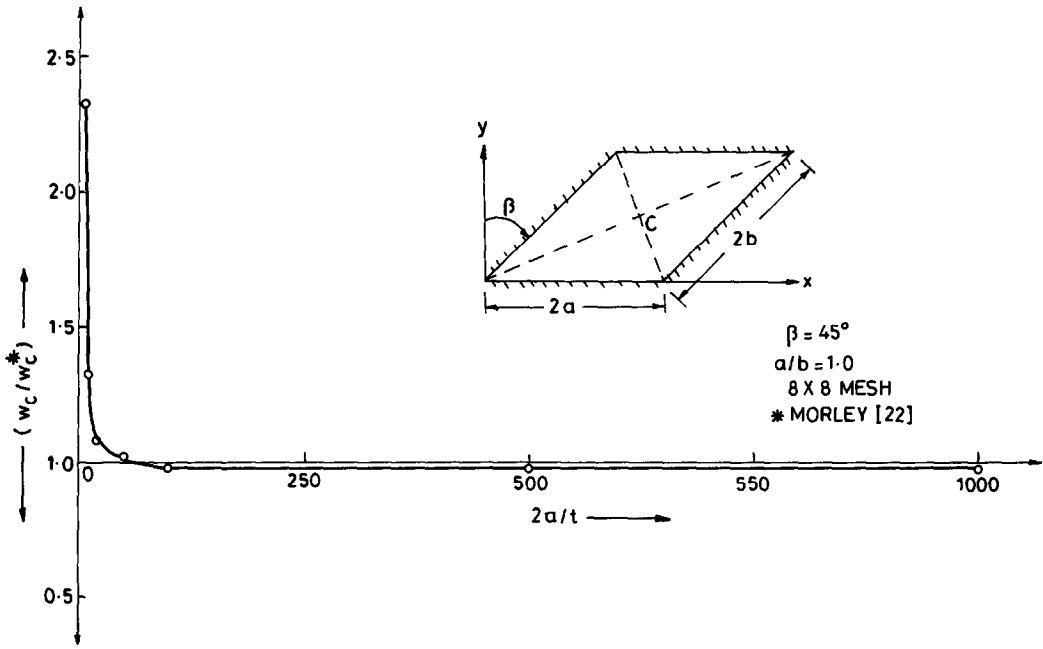
Fig. 7. Locking test for 45° skew clamped plate under uniformly distributed load.
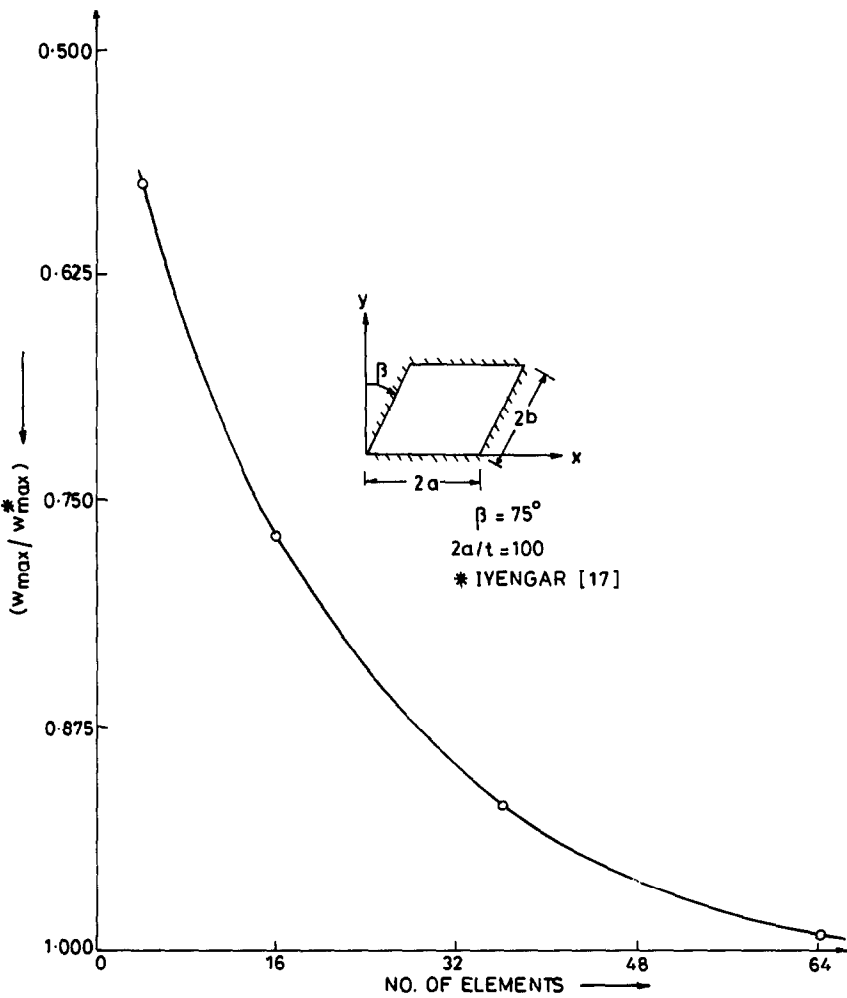
Fig. 8. Convergence of centre deflection with mesh refinement for a 75° skew clamped plate under uniformly distributed load.

Table 1. Clamped skew plate under uniformly distributed loading

Skew angle β		$w_{max}=\alpha_1\cdot\dfrac{qa^4}{D}\cdot10^{-2}$ α_1	$M_{ppl\,max}=\alpha_2\cdot qa^2\cdot10^{-2}$ α_2	$M_{ppl\,min}=\alpha_3\cdot qa^2\cdot10^{-2}$ α_3	$Q_{x1}=\alpha_4\cdot qa\cdot10^{-1}$ α_4	$Q_{y1}=\alpha_5\cdot qa\cdot10^{-1}$ α_5	$Q_{x2}=\alpha_6\cdot qa\cdot10^{-1}$ α_6	$Q_{y2}=\alpha_7\cdot qa\cdot10^{-1}$ α_7
15°	Present	1.7948	9.2207	8.1785	7.0056	−2.2866	−0.3955	7.3584
	Iyengar and Srinivasan [17]	1.7968	9.2520	—	—	—	—	—
	Ramesh et al. [41]	1.7950	—	—	—	—	—	—
	Morley [72]	1.7968	—	—	—	—	—	—
	Morley [71]	—	9.2520	—	—	—	—	—
30°	Present	1.2281	7.9906	6.2273	4.4008	−3.1125	−0.4951	5.3673
	Iyengar and Srinivasan [17]	1.2299	8.0000	—	—	—	—	—
	Ramesh et al. [41]	1.2258	—	—	—	—	—	—
	Morley [72]	1.2304	—	—	—	—	—	—
	Gangarao and Chaudhary [21]	1.2304	—	—	—	—	—	—
	Morley [71]	—	8.0000	—	—	—	—	—
	Argyris [30]	—	8.0800	—	—	—	—	—
45°	Present	0.5997	5.8270	3.8933	2.0429	−2.4460	−0.2850	3.1741
	Iyengar and Srinivasan [17]	0.6018	—	—	—	—	—	—
	Ramesh et al. [41]	0.5952	—	—	—	—	—	—
	Morley [72]	0.6032	—	—	—	—	—	—
	Morley [71]	—	5.7600	—	—	—	—	—
60°	Present	0.1704	3.2603	1.7639	0.9031	−1.7306	−0.0832	1.9504
	Iyengar and Srinivasan [17]	0.1717	—	—	—	—	—	—
	Ramesh et al. [41]	0.1638	—	—	—	—	—	—
	Gangarao and Chaudhary [21]	0.1728	—	—	—	—	—	—
75°	Present	0.0143	0.9998	0.3942	0.3007	−1.2397	−0.0304	1.2753
	Iyengar and Srinivasan [17]	0.0144	—	—	—	—	—	—
	Ramesh et al. [41]	0.0120	—	—	—	—	—	—

$[w/(Qa^2/D)] \times 10^2$

Fig. 10. Deflection profile for clamped skew plate under central concentrated load.

$[w/(qa^4/D)] \times 10^2$

Fig. 9. Deflection profile for clamped skew plate under uniformly distributed load.

Table 2. Clamped skew plate under central concentrated load

Skew angle β		$w_{max} = \alpha_1 \cdot \frac{Qa^2}{D} \cdot 10^{-2}$	$M_{ppl\,max} = \alpha_2 \cdot Q \cdot 10^{-1}$	$M_{ppl\,min} = \alpha_3 \cdot Q \cdot 10^{-1}$	$Q_{x1} = \alpha_4 \cdot \frac{Q}{a} \cdot 10^{-1}$	$Q_{y1} = \alpha_5 \cdot \frac{Q}{a} \cdot 10^{-1}$	$Q_{x2} = \alpha_6 \cdot \frac{Q}{a} \cdot 10^{-1}$	$Q_{y2} = \alpha_7 \cdot \frac{Q}{a} \cdot 10^{-1}$
		α_1	α_2	α_3	α_4	α_5	α_6	α_7
15°	Present	2.0955	3.1578	2.7720	0.6973	-0.4768	-0.2801	0.7968
	Morley [72]	2.108	—	—	—	—	—	—
30°	Present	1.7030	3.1076	2.4052	-1.4410	0.8101	0.0189	-1.6531
	Morley [72]	1.732	—	—	—	—	—	—
45°	Present	1.1481	2.8969	1.9720	-2.0484	3.0757	0.7264	-3.6233
	Morley [72]	1.196	—	—	—	—	—	—
60°	Present	0.5635	2.5044	1.4437	0.2976	1.4714	0.9934	-1.1255
75°	Present	0.1211	1.7170	0.7307	1.2897	-3.8068	0.2605	4.0107

Table 3. Cantilever skew plate under uniformly distributed loading

Skew angle β		$w_3 = \alpha_1 \cdot \frac{qa^4}{D}$	$w_4 = \alpha_2 \cdot \frac{qa^4}{D}$	$M_{ppl\,max} = \alpha_3 \cdot qa^2$	$M_{ppl\,min} = \alpha_4 \cdot qa^2$	$Q_{x1} = \alpha_5 \cdot qa$	$Q_{y1} = \alpha_6 \cdot qa$
		α_1	α_2	α_3	α_4	α_5	α_6
15°	Present	2.1182	1.6848	-1.9798	-0.5939	2.4549	-1.7365
30°	Present	1.9375	1.1601	-1.4708	-0.4412	1.3598	-2.7152
45°	Present	1.5893	0.6229	-0.7987	-0.2396	0.2490	-2.6764
60°	Present	1.2006	0.2231	-0.2303	-0.0689	-0.3380	-2.2066
	Monforton and Schmitz [37]	1.1936	0.2240	—	—	—	—
	Yettram [81]	1.1440	0.2000	-0.1620	-0.0348	—	—
	*Veubeke [81]	—	—	-0.2220	-0.0660	—	—
75°	Present	0.8651	0.0306	-0.0297	-0.0081	-0.4349	-1.2062

* Taken from Ref. [81].

Table 4. Cantilever skew plate under concentrated load at centre of free edge

Skew angle β		$w_3 = \alpha_1 \cdot \frac{Qa^2}{D}$	$w_4 = \alpha_2 \cdot \frac{Qa^2}{D}$	$M_{ppl\,max} = \alpha_3 \cdot Q \cdot 10^{-1}$	$M_{ppl\,min} = \alpha_4 \cdot Q \cdot 10^{-1}$	$Q_{x1} = \alpha_5 \cdot \frac{Q}{a}$	$Q_{y1} = \alpha_6 \cdot \frac{Q}{a}$
		α_1	α_2	α_3	α_4	α_5	α_6
15°	Present	1.4554	1.4044	-10.752	-3.2255	0.8483	-1.0419
30°	Present	1.5369	1.2890	-8.2947	-2.4883	0.1185	-1.6388
45°	Present	1.6079	1.1365	-4.5030	-1.3508	-0.5592	-1.7207
60°	Present	1.7822	1.0135	-0.5381	-0.1381	-0.8252	-2.1605
75°	Present	2.5217	1.1128	-0.4529	0.0934	-1.3133	-2.8361
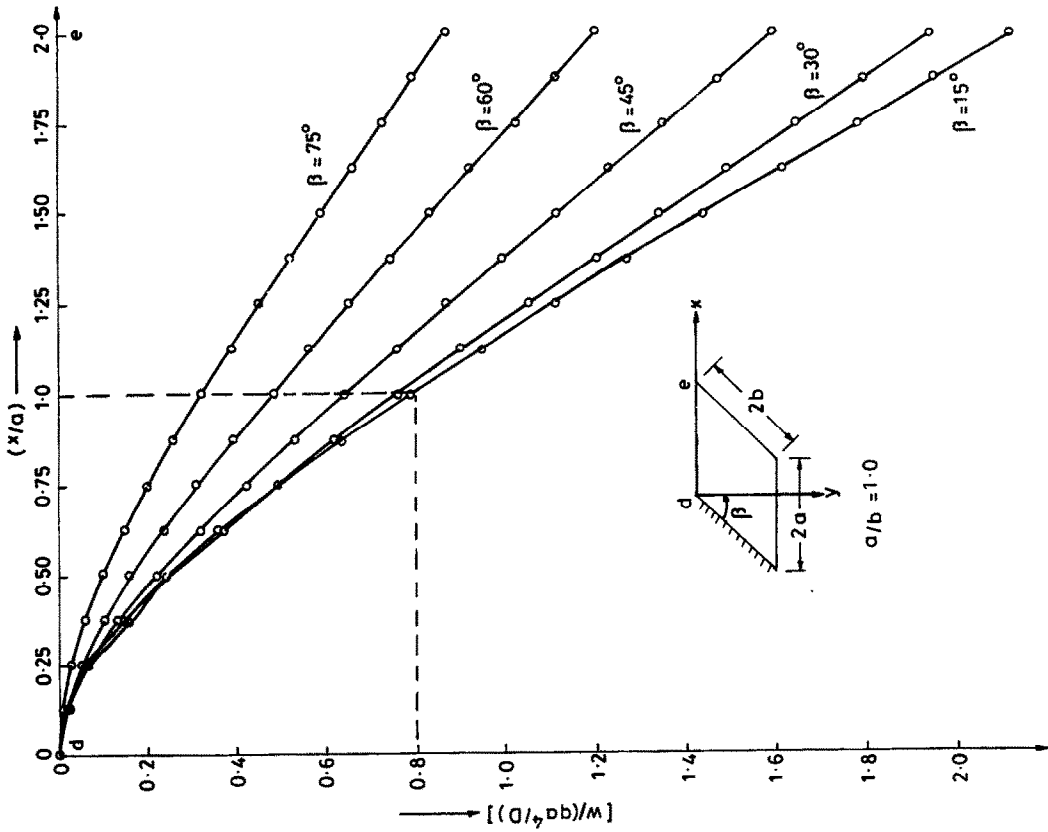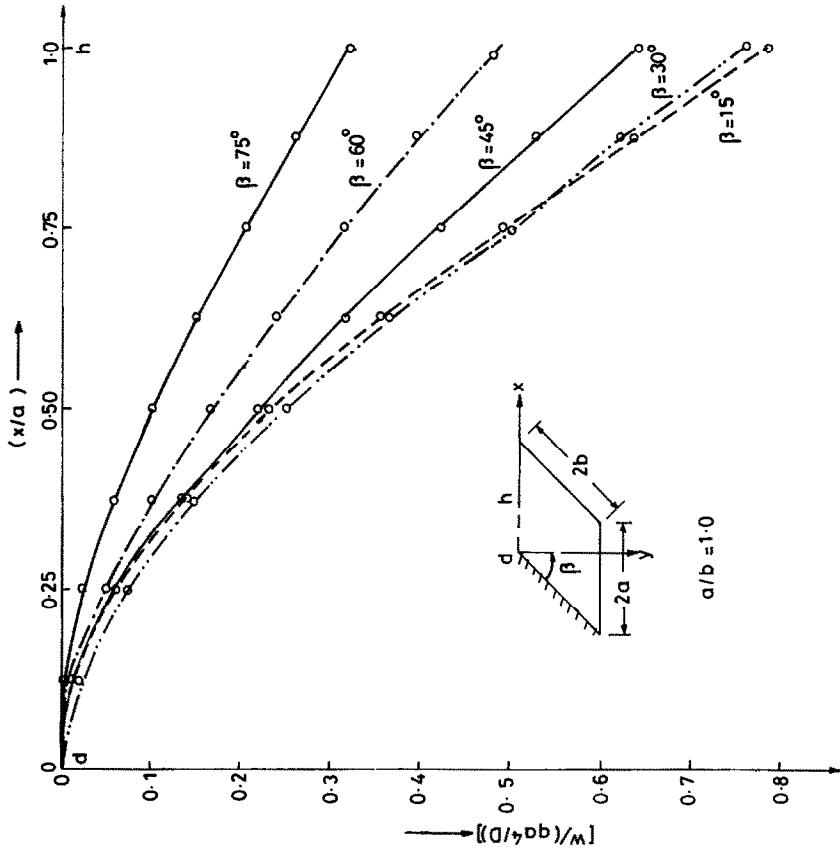
Fig. 12. Deflection profile (enlarged) for cantilever skew plate under uniformly distributed load.

Fig. 11. Deflection profile for cantilever skew plate under uniformly distributed load.
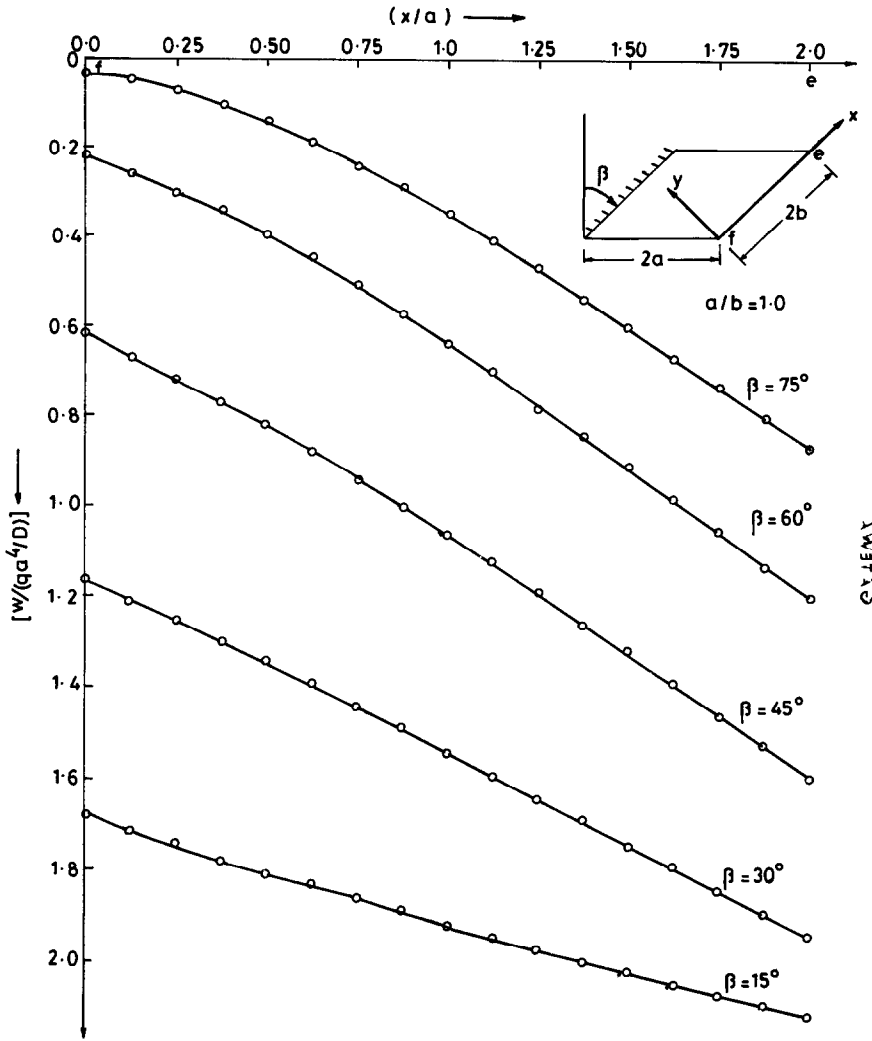
Fig. 13. Deflection profile for cantilever skew plate under uniformly distributed load.

Example 4

Cantilever skew plate: a cantilever skew plate having side AB (see Fig. 4) as clamped (CL) for various skew angles is analysed under uniformly distributed load and concentrated load at the centre of free edge CD (see Fig. 4). Deflection at points 3 and 4, principal bending moments as well as shear forces at the centre of the clamped edge are presented in Tables 3 and 4.

For a uniformly loaded cantilever skew plate limited comparison for only 60° skew angle was found in the literature, which shows good agreement. Deflection profiles along sections 'de', 'dh' and 'ef' are shown in Figs 11–13 respectively. However, no results are reported in literature for concentrated load at the centre of free edge CD. Deflection profiles along sections 'd'e'' and 'g'f'' are shown in Figs 14 and 15 respectively.

Example 5

Skew plate clamped on two opposite sides: a skew

plate clamped (CL) on sides BC and AD (Fig. 4) was analysed for various skew angles under uniformly distributed as well as centrally concentrated load. Central deflection, principal bending moments at centre as well as shear forces at points 1 and 2 are presented in Tables 5 and 6. Deflection profiles along 'de' for uniformly distributed and concentrated load are shown in Figs 16 and 17, respectively. However, no results are available in literature for comparison.

Example 6

Skew plate simply supported on two opposite sides: a skew plate simply supported (SS1 as well as SS2) on sides BC and AD (Fig. 4) was analysed for various skew angles under uniformly distributed as well as central concentrated load. Central deflection, principal bending moments at centre as well as shear forces at points 1 and 2 (Fig. 4) are presented in Tables 7 and 8.

For uniformly distributed load, reasonable accuracy is achieved for the limited results for central
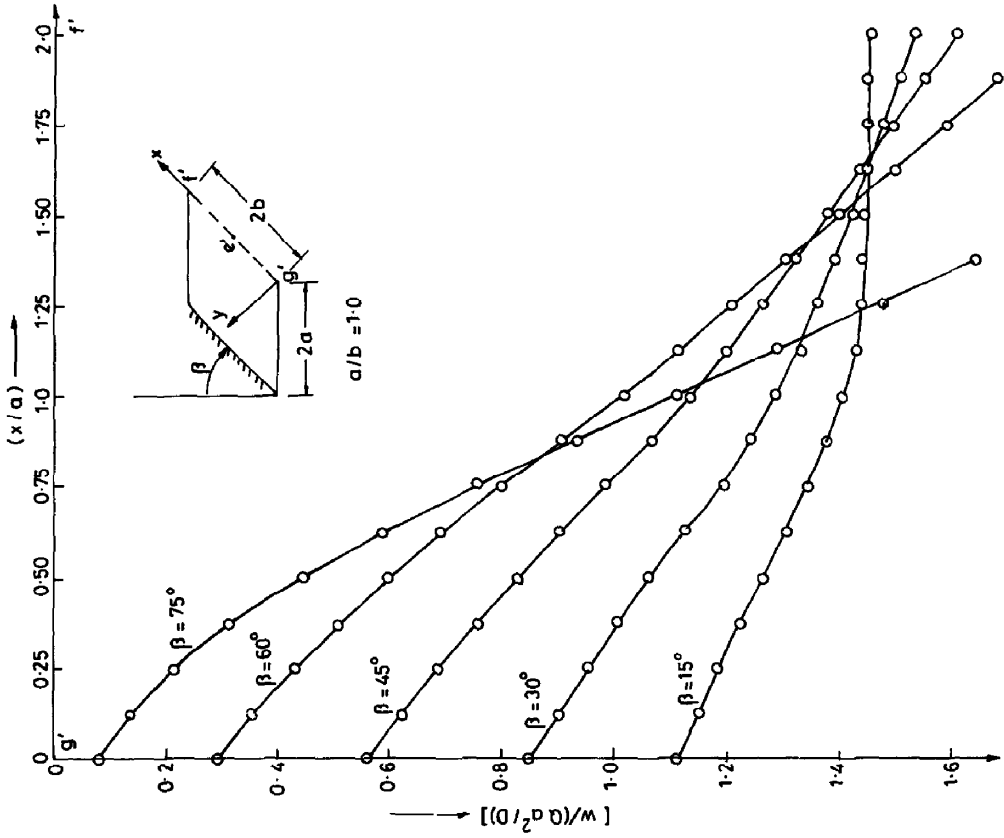
Fig. 15. Deflection profile for cantilever skew plate under concentrated load at centre of free edge (e').
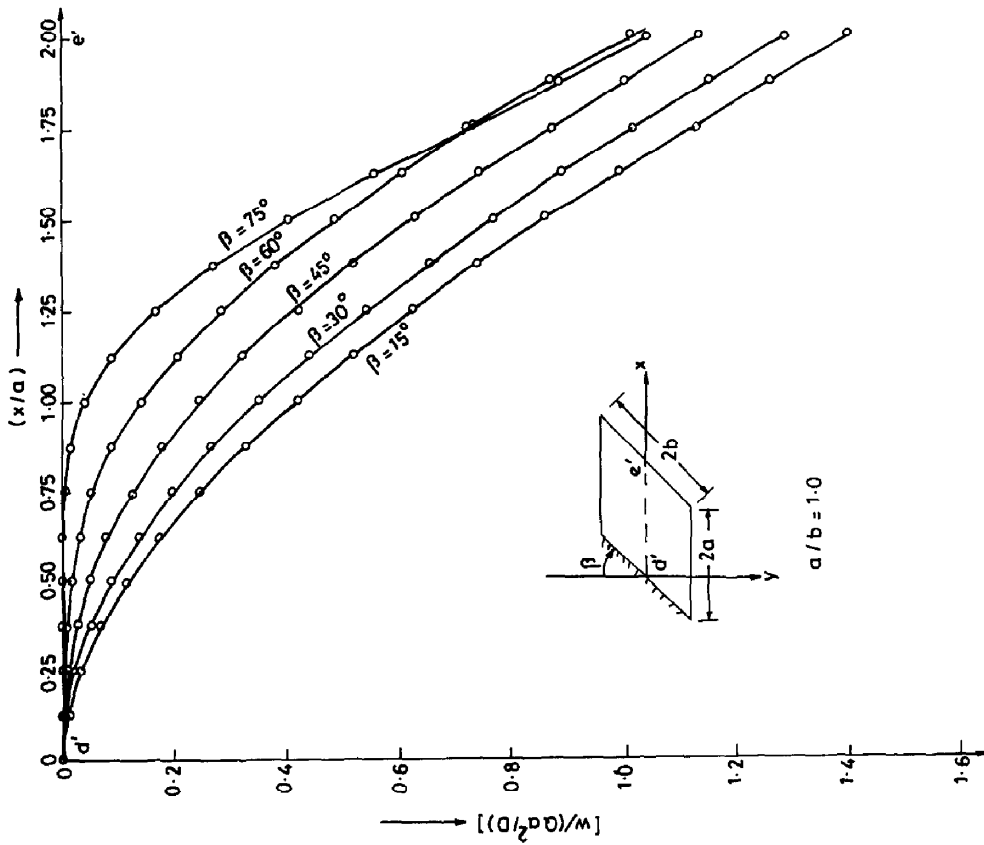
Fig. 14. Deflection profile for cantilever skew plate under concentrated load at centre of free edge (e').

Table 5. Skew plate with two opposite edges clamped under uniformly distributed loading

Skew angle β		$w_0 = \alpha_1 \cdot \frac{qa^4}{D} \cdot 10^{-2}$	$M_{ppl\,max} = \alpha_2 \cdot qa^2 \cdot 10^{-2}$	$M_{ppl\,min} = \alpha_3 \cdot qa^2 \cdot 10^{-2}$	$Q_{x1} = \alpha_4 \cdot qa \cdot 10^{-1}$	$Q_{y1} = \alpha_5 \cdot qa \cdot 10^{-1}$	$Q_{x2} = \alpha_6 \cdot qa \cdot 10^{-1}$	$Q_{y2} = \alpha_7 \cdot qa \cdot 10^{-1}$
		α_1	α_2	α_3	α_4	α_5	α_6	α_7
15°	Present	3.6395	15.764	3.9226	0.00723	-1.1394	-0.7236	9.8646
30°	Present	2.4974	13.252	2.4302	0.3372	-0.9822	-1.1428	9.5704
45°	Present	1.2271	9.5230	0.7217	2.0209	0.5828	-1.2402	8.9454
60°	Present	0.3488	5.1965	-0.3062	4.6164	2.1675	-1.2159	7.3487
75°	Present	0.0276	1.4890	-0.1525	3.2382	1.6404	-0.6003	2.8997

Table 6. Skew plate with two opposite edges clamped under central concentrated load

Skew angle β		$w_0 = \alpha_1 \cdot \frac{Qa^2}{D} \cdot 10^{-1}$	$M_{ppl\,max} = \alpha_2 \cdot Q \cdot 10^{-1}$	$M_{ppl\,min} = \alpha_3 \cdot Q \cdot 10^{-1}$	$Q_{x1} = \alpha_4 \cdot \frac{Q}{a} \cdot 10^{-2}$	$Q_{y1} = \alpha_5 \cdot \frac{Q}{a} \cdot 10^{-2}$	$Q_{x2} = \alpha_6 \cdot \frac{Q}{a} \cdot 10^{-2}$	$Q_{y2} = \alpha_7 \cdot \frac{Q}{a} \cdot 10^{-2}$
		α_1	α_2	α_3	α_4	α_5	α_6	α_7
15°	Present	2.8559	3.3691	2.7930	-9.5106	-13.883	-4.5739	23.274
30°	Present	2.3078	3.2970	2.4442	-14.879	-18.689	-4.3653	5.0361
45°	Present	1.5463	3.0856	2.0161	-16.341	-9.7852	0.6643	-11.756
60°	Present	0.7590	2.6919	1.4994	-9.5179	5.7626	5.3183	-3.8849
75°	Present	0.1674	1.8778	0.7995	4.0787	-3.1702	2.4573	39.259
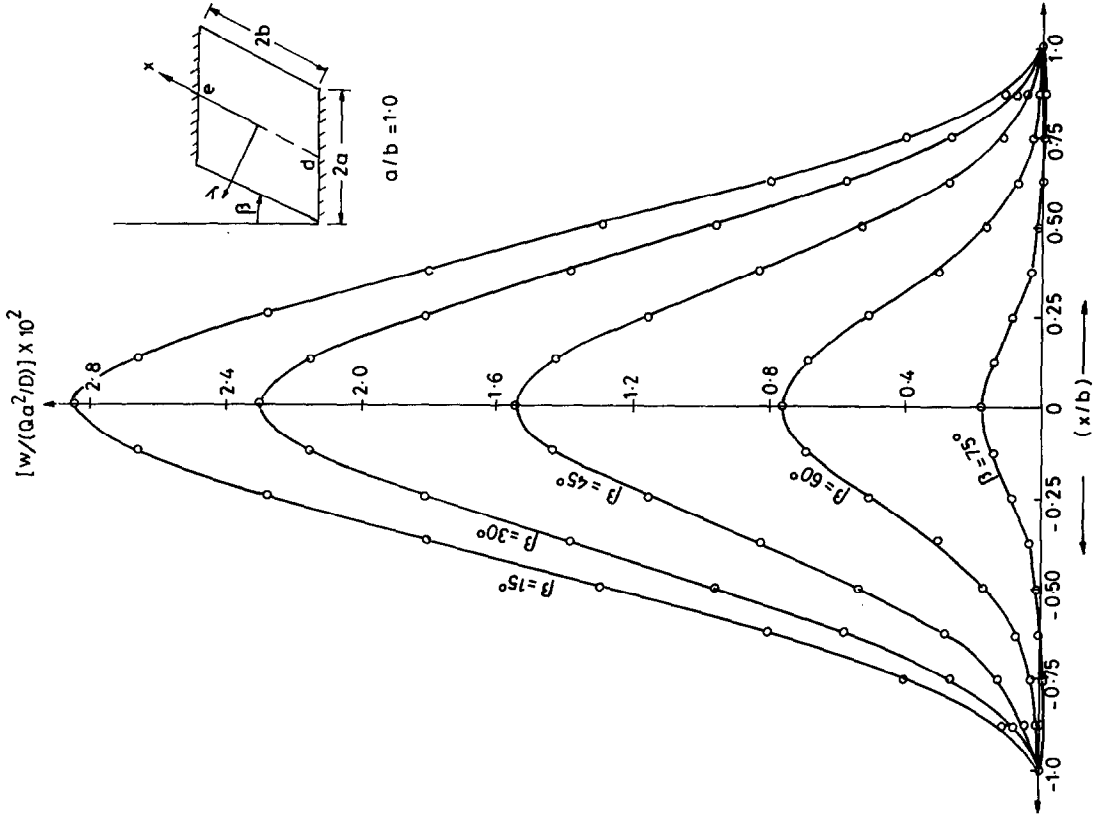
Fig. 17. Deflection profile for skew plate clamped on two opposite edges under central concentrated load.
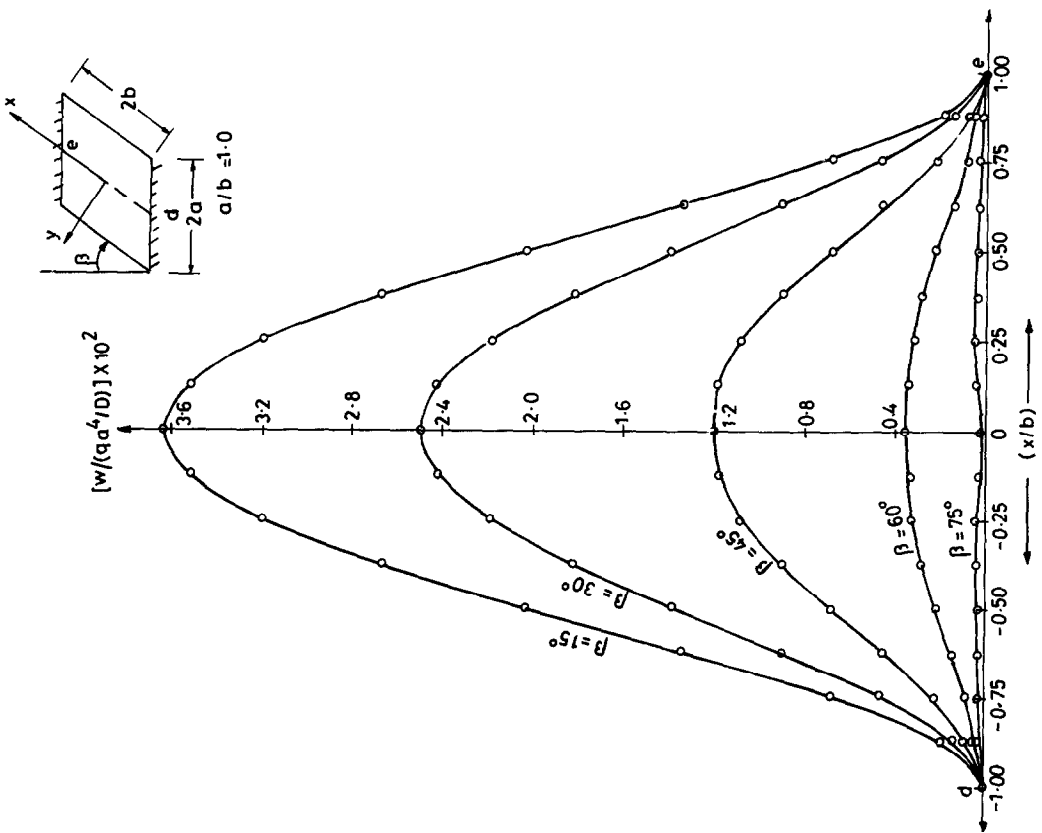
Fig. 16. Deflection profile for skew plate clamped on two opposite edges under uniformly distributed load.

Table 7. Skew plate with two opposite edges simply supported (SS1 and SS2) under uniformly distributed loading

Skew angle β		$w_0 = \alpha_1 \cdot \dfrac{Qa^4}{D} \cdot 10^{-1}$	$M_{ppl\,max} = \alpha_2 \cdot qa^2 \cdot 10^{-1}$	$M_{ppl\,min} = \alpha_3 \cdot qa^2 \cdot 10^{-1}$	$Q_{x1} = \alpha_4 \cdot qa$	$Q_{y1} = \alpha_5 \cdot qa$	$Q_{x2} = \alpha_6 \cdot qa \cdot 10^{-1}$	$Q_{y2} = \alpha_7 \cdot qa \cdot 10^{-1}$
		α_1	α_2	α_3	α_4	α_5	α_6	α_7
15°	Present (SS2)	1.8556	4.6664	0.9759	−0.2157	−1.2923	0.4968	7.2196
	Present (SS1)	1.8556	4.6652	0.9660	−0.3542	−1.2858	1.3546	7.2182
30°	Present (SS2)	1.2679	3.9094	0.6446	−0.8711	−1.8725	0.5741	5.5417
	Present (SS1)	1.2680	3.9094	0.6355	−1.0220	−1.8633	4.2407	5.5344
	Crisfield [59]	1.2687	—	—	—	—	—	—
	Jirousek and Leon [68]	1.2549	—	—	—	—	—	—
	Razzaque [28]	1.2712	—	—	—	—	—	—
	Yettram [81]	1.2422	—	—	—	—	—	—
45°	Present (SS2)	0.6287	2.8329	0.2148	−1.3076	−1.5602	0.0839	3.5641
	Present (SS1)	0.6287	2.8340	0.2073	−1.4422	−1.5531	9.7605	3.6389
60°	Present (SS2)	0.1900	1.6357	−0.1386	−1.2938	−0.8120	−1.4359	3.6098
	Present (SS1)	0.1899	1.6363	−0.1443	−1.3672	−0.8123	15.830	3.8660
	Timoshenko and Woinowsky-Krieger [29]	0.1860	—	—	—	—	—	—
	Yettram [81]	0.1853	—	—	—	—	—	—
75°	Present (SS2)	0.0183	0.5413	−0.2053	−1.2860	−0.2529	−2.1791	8.4529
	Present (SS1)	0.0182	0.5381	−0.2114	−1.3193	−0.2638	15.575	8.7949

Table 8. Skew plate with two opposite edges simply supported (SS1 and SS2) under central concentrated load

Skew angle β		$w_0 = \alpha_1 \cdot \frac{Qa^2}{D} \cdot 10^{-2}$	$M_{ppl\,max} = \alpha_2 \cdot Q \cdot 10^{-1}$	$M_{ppl\,min} = \alpha_3 \cdot Q \cdot 10^{-1}$	$Q_{x1} = \alpha_4 \cdot \frac{Q}{a} \cdot 10^{-1}$	$Q_{y1} = \alpha_5 \cdot \frac{Q}{a} \cdot 10^{-1}$	$Q_{x2} = \alpha_6 \cdot \frac{Q}{a} \cdot 10^{-1}$	$Q_{y2} = \alpha_7 \cdot \frac{Q}{a} \cdot 10^{-1}$
		α_1	α_2	α_3	α_4	α_5	α_6	α_7
15°	Present (SS2)	8.5811	4.5126	3.1847	-1.5369	-4.8685	-0.4472	2.2918
	Present (SS1)	8.5822	4.5141	3.1884	-1.6179	-4.8483	-4.0084	2.3712
	Robinson [25]	9.2778	—	—	—	—	—	—
30°	Present (SS2)	6.7170	4.3567	2.8522	-4.1081	-7.3134	-0.1929	1.2197
	Present (SS1)	6.7189	4.3575	2.8536	-4.2862	-7.2830	-6.6582	1.2826
	Robinson [25]	7.2483	—	—	—	—	—	—
45°	Present (SS2)	4.2925	4.0659	2.4145	-5.8588	-5.8883	0.9556	-0.8968
	Present (SS1)	4.2950	4.0664	2.4129	-6.1046	-5.8561	-6.3942	-0.9048
	Robinson [25]	4.6237	3.7000	2.5700	—	—	—	—
	Argyris [30]	4.2400	4.4300	2.3700	—	—	—	—
	Morley [22]	4.6800	3.7000	2.5700	—	—	—	—
60°	Present (SS2)	2.0043	3.5939	1.8776	-4.2399	-1.1850	3.0466	-3.3084
	Present (SS1)	2.0066	3.5952	1.8792	-4.4013	-1.1501	-3.2744	-3.4366
	Robinson [25]	2.1492	—	—	—	—	—	—
75°	Present (SS2)	0.4393	2.6898	1.1241	0.1128	0.8698	0.3782	1.9133
	Present (SS1)	0.4402	2.6931	1.1279	0.1099	0.8821	0.1553	1.8650
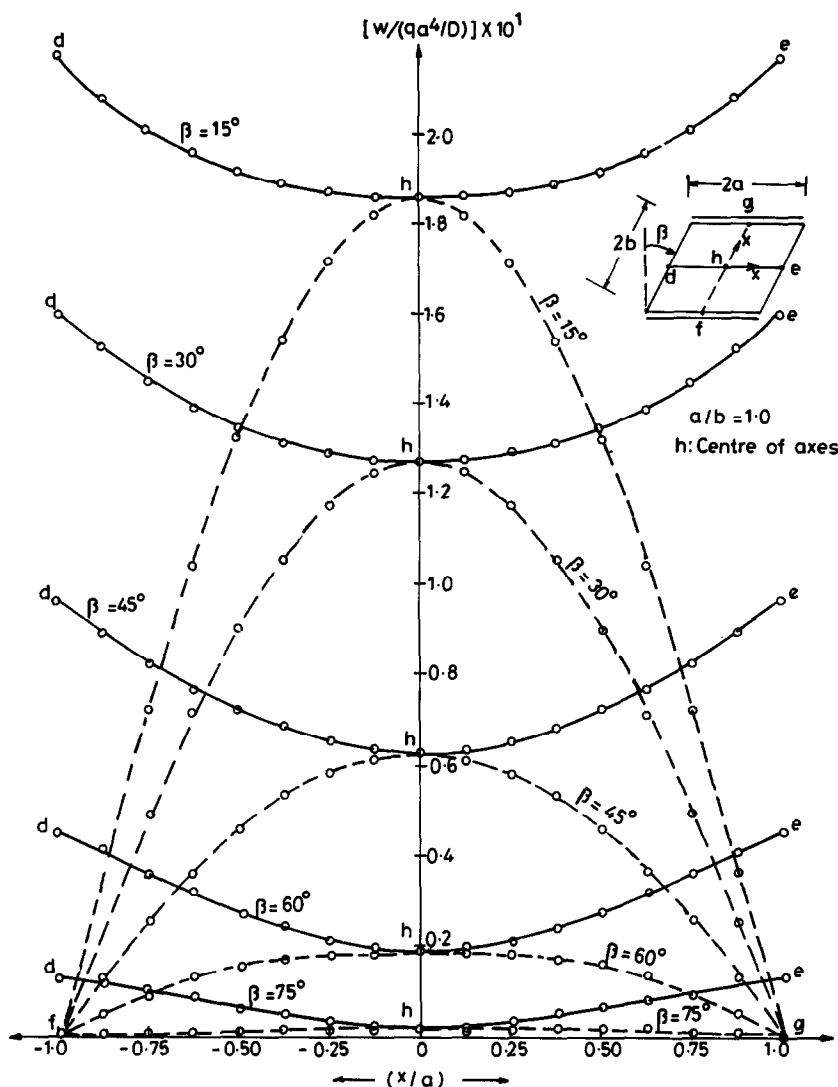
Fig. 18. Deflection profile for skew plate simply supported on two opposite edges under uniformly distributed load.

deflection reported in the literature. Deflection profiles along sections 'de' and 'fg' are shown for the SS2 boundary condition in Fig. 18. For central concentrated load, agreement with other reported values is satisfactory. Deflection profiles along sections 'de' and 'fg' are shown for the SS2 boundary condition in Fig. 19.

Example 7

Skew plate having all sides simply supported: a skew plate simply supported (SS2) on all edges AB, BC, CD and AD, except at points A, B, C, D (Fig. 4) where it is just supported (SS1), was analysed for various skew angles under uniformly distributed as well as central concentrated load. Maximum central deflection, principal bending moments at centre as well as shear forces at points 1 and 2 (Fig. 4) are presented in Tables 9 and 10.

For uniformly loaded plate, good agreement is achieved up to $\beta = 45°$, but beyond this skew angle

solution seems to be overstiff. For $\beta = 60°$, the calculated central deflection is 79.56% of Morley's [22] analytical value. To improve the results the 8 × 8 skew mesh may be refined further but a better option would be to redefine the mesh pattern as a 'special mesh' as shown in Fig. 5b and c. A detailed comparison is carried out in Example 8. Deflection profiles along section 'de' are shown in Fig. 20.

Even for central concentrated load, the above discussion holds true qualitatively. In fact, beyond a skew angle of 30°, results are in large error. Deflection profiles along section 'de' are shown in Fig. 21.

Example 8

Morley's acute skew plate problem: the 60° skew Morley's rhombic plate poses a stringent test for all plate bending elements. The parameters adopted for analysis are shown in Fig. 22. Only one quadrant 'ocf' is analysed under uniformly distributed load for
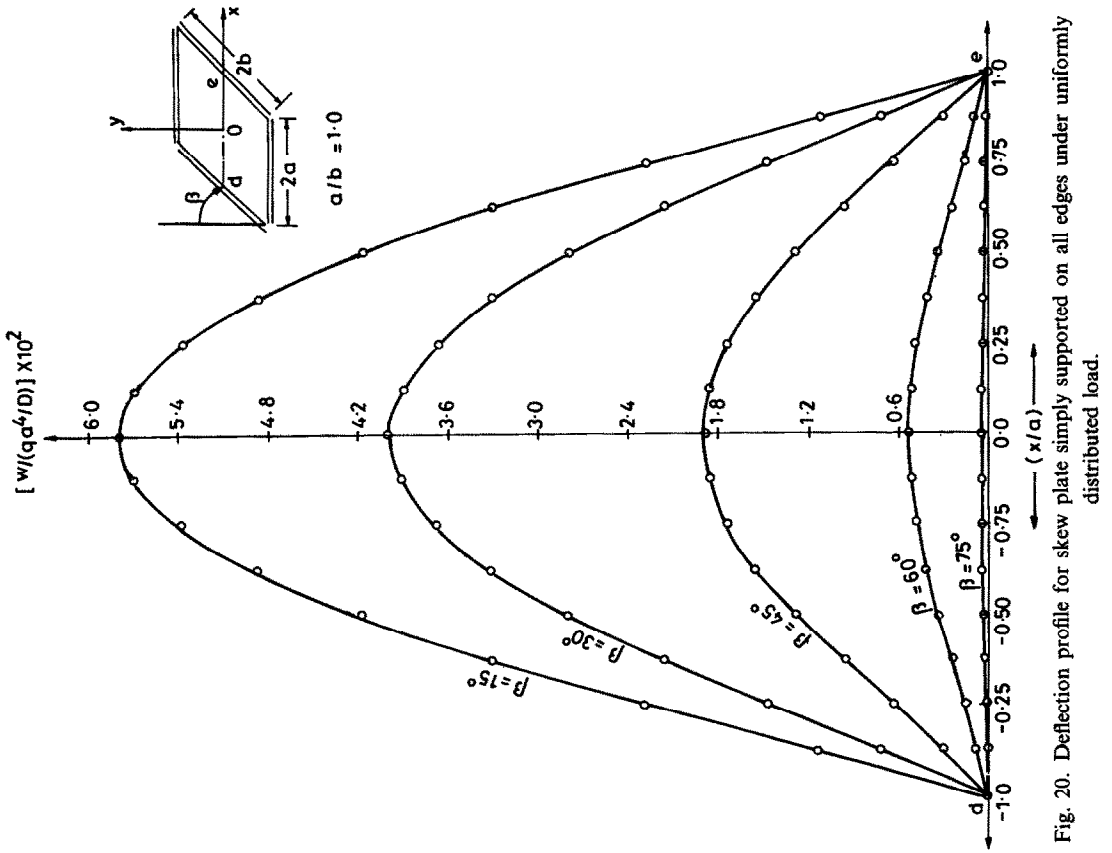
Fig. 20. Deflection profile for skew plate simply supported on all edges under uniformly distributed load.
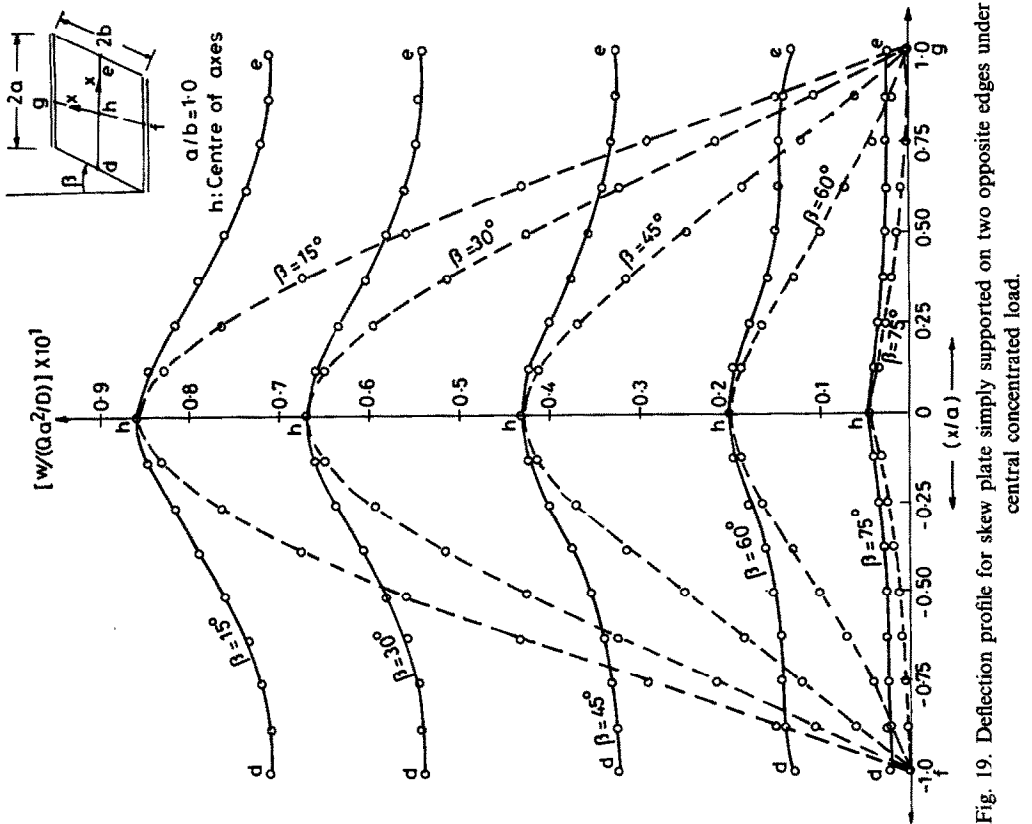
Fig. 19. Deflection profile for skew plate simply supported on two opposite edges under central concentrated load.

Table 9. Skew plate with all edges simply supported (SS2) under uniformly distributed loading

Skew angle β		$w_{max} = \alpha_1 \cdot \dfrac{qa^4}{D} \cdot 10^{-2}$	$M_{pplmax} = \alpha_2 \cdot qa^2 \cdot 10^{-1}$	$M_{pplmin} = \alpha_3 \cdot qa^2 \cdot 10^{-1}$	$Q_{x1} = \alpha_4 \cdot qa \cdot 10^{-1}$	$Q_{y1} = \alpha_5 \cdot qa \cdot 10^{-1}$	$Q_{x2} = \alpha_6 \cdot qa \cdot 10^{-1}$	$Q_{y2} = \alpha_7 \cdot qa \cdot 10^{-1}$
		α_1	α_2	α_3	α_4	α_5	α_6	α_7
15°	Present	5.8013	1.9207	1.7082	7.2798	-4.1571	-2.1350	8.1067
	GangaRao and Chaudhary [21]	5.8240	—	—	—	—	—	—
30°	Present	3.9832	1.6790	1.2980	5.4165	-6.4599	-2.8856	7.9202
	Morley [22]	4.0960	1.7000	1.3320	—	—	—	—
	GangaRao and Chaudhary [21]	4.0960	—	—	—	—	—	—
45°	Present	1.9125	1.2266	0.7803	3.3924	-5.9064	-1.7777	6.5752
	GangaRao and Chaudhary [21]	2.1120	—	—	—	—	—	—
	Argyris [30]	2.0787	1.2983	0.8570	—	—	—	—
60°	Present	0.5194	0.6662	0.3166	1.5958	-3.1333	-0.1848	3.5117
	Morley [22]	0.6528	0.7640	0.4320	—	—	—	—
	GangaRao and Cahudhary [21]	0.6496	—	—	—	—	—	—
	Argyris [30]	0.6158	0.7668	0.4028	—	—	—	—
	Rossow [95]	0.6526	0.7625	0.4343	—	—	—	—
	Jirousek [69]	0.6526	—	—	—	—	—	—
75°	Present	0.0422	0.1906	0.0639	0.3155	-0.6109	0.1467	0.6722

Table 10. Skew plate with all edges simply supported (SS2) under central concentrated load

Skew angle β		$w_{max} = \alpha_1 \cdot \dfrac{Qa^2}{D} \cdot 10^{-2}$	$M_{pplmax} = \alpha_2 \cdot Q \cdot 10^{-1}$	$M_{pplmin} = \alpha_3 \cdot Q \cdot 10^{-1}$	$Q_{x1} = \alpha_4 \cdot \dfrac{Q}{a} \cdot 10^{-1}$	$Q_{y1} = \alpha_5 \cdot \dfrac{Q}{a} \cdot 10^{-1}$	$Q_{x2} = \alpha_6 \cdot \dfrac{Q}{a} \cdot 10^{-1}$	$Q_{y2} = \alpha_7 \cdot \dfrac{Q}{a}$
		α_1	α_2	α_3	α_4	α_5	α_6	α_7
15°	Present	4.3524	3.7142	3.2950	1.9934	-2.1501	-1.5630	2.4814
	Aggarwal [79]	4.3555	—	—	—	—	—	—
30°	Present	3.5216	3.6722	2.8920	0.9867	-2.6744	-1.8223	2.1914
	Aggarwal [79]	3.6000	—	—	—	—	—	—
	Vora and Matlock [43]	3.7560	—	—	—	—	—	—
45°	Present	2.3088	3.4467	2.3850	0.5239	-0.6257	-0.0720	0.8128
	Aggarwal [79]	2.5094	—	—	—	—	—	—
60°	Present	1.0729	2.9839	1.7420	0.9135	2.7004	2.1412	-1.8816
	Argyris [30]	1.2442	—	—	—	—	—	—
75°	Present	0.2285	2.0845	0.9127	0.9643	-0.0600	0.9159	0.3075
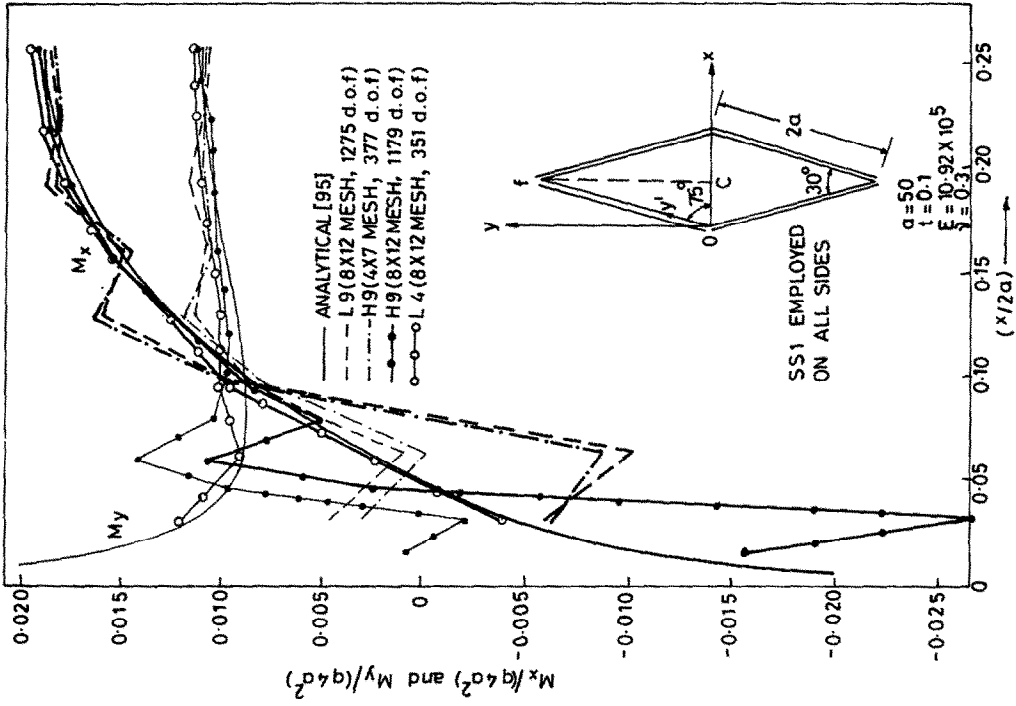
Fig. 22. Morley's acute skew plate: bending moment distribution along OC.
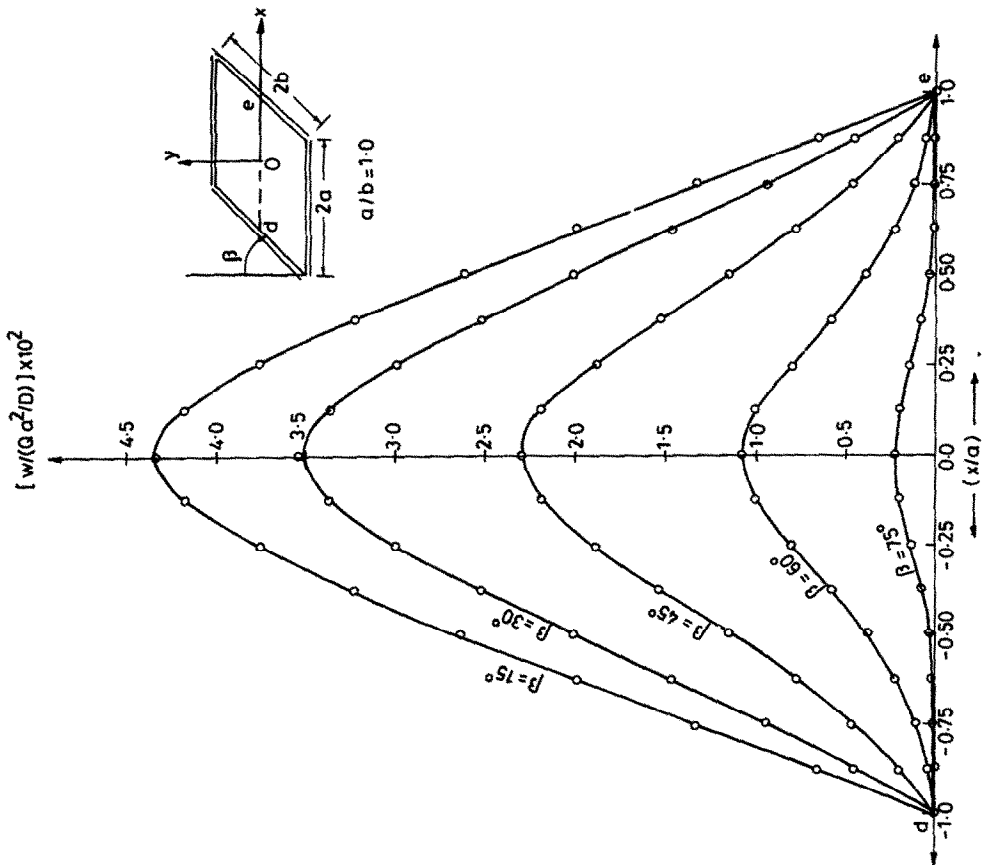
Fig. 21. Deflection profile for skew plate simply supported on all edges under central concentrated load.

Table 11. Morley's acute skew plate ($\beta = 60°$) under uniformly distributed loading

Element	Mesh per quadrant	Degrees of freedom per quadrant	Boundary conditions employed		$w_{max} = \alpha_1 \cdot \dfrac{qa^4}{D} \cdot 10^{-2}$	$M_{ppl\,max} = \alpha_2 \cdot qa^2 \cdot 10^{-2}$	$M_{ppl\,min} = \alpha_3 \cdot qa^2 \cdot 10^{-2}$
			On sides	At obtuse corner	α_1	α_2	α_3
H9	4 × 4 non-refined	227	SS1	$w = 0$	0.5779	5.9155	3.7225
H9	8 × 12 non-refined	1179	SS2	$w = \theta_s = 0$	0.6475	7.6623	4.3710
H9	8 × 12 non-refined	1179	SS1	$w = 0$	0.6510	7.8035	4.6883
H9	4 × 4 non-refined	227	SS1	$w = 0$	0.5893	5.8333	3.7968
H9	4 × 7 refined	377	SS1	$w = 0$	0.6487	7.5773	4.3028
H9	8 × 12 non-refined	1179	SS1	$w = 0$	0.6545	7.7400	4.4355
H9	8 × 12 refined	1179	SS1	$w = 0$	0.6580	7.6305	4.2193
L9	8 × 12 refined	1275	SS1	$w = 0$	0.6481	7.3128	4.3100
L4	8 × 12 refined	351	SS1	$w = 0$	0.6788	7.8288	4.5510
Morley [22]	—	—	—	—	0.6528	7.6400	4.3200

various types of elements, namely four-node Lagrange (L4), nine-node Lagrange (L9) and nine-node Heterosis (H9), for different types of special mesh patterns and sizes. The boundary conditions adopted are explicitly mentioned in Table 11, which gives the values of central deflection and principal bending moments at the centre of the plate. All the results have been compared with Morley's [22] analytical solution. A special mesh pattern is adopted which may or may not be refined as indicated in Fig. 5b and c. It is observed that results are highly sensitive to the boundary conditions adopted at the obtuse corner. The comparison of skew and special mesh results for this problem indicates the superiority of the latter. The refined special mesh in fact gives the best results. The best results for central deflection and principal moments are achieved using the H9 element with an 8 × 12 refined special mesh adopting the SS1 boundary conditions on the sides of the plate. The adoption of SS1 or SS2 boundary conditions does not affect the results considerably.

The moments M_x and M_y are strongly singular in nature in the vicinity of the obtuse vertices but are of opposite signs. The moments vary asymptotically as $(r)^{-4/5}$, where r is the distance from the obtuse vertex [95]. This singularity problem has been discussed in detail in the literature [22, 44, 52, 54, 60, 62, 69, 95], yet most finite element methods either fail to converge or converge very slowly to this singular behaviour. Thus, using the refined special mesh as shown in Fig. 5c, moments M_x and M_y were plotted along the shorter diagonal 'oc' for H9, L9 and L4 elements for various mesh sizes. Graphical results are shown in Fig. 22. The L4 element with a total of 351 degrees of freedom behaved the best, while the L9 element with a total of 1275 degrees of freedom could not model the singularity adequately and the Heterosis (H9) element, even with a total of 1179 degrees of freedom, behaved the worst. The oscillations near the obtuse vertex for H9 element in fact increased as total degrees of freedom were increased from 377 to 1179. Such an erratic behaviour of the Heterosis element is quite surprising.

However, from the above discussion it is evident that, using the H9 element, as the mesh size is reduced, central deflection as well as principal bending moments at the centre converge rapidly but obtuse corner modelling rather deteriorates. In comparison the L4 element behaves much better for obtuse corner modelling even at one-third the total degrees of freedom of that for H9.

CONCLUSIONS

The performance of the nine-node Heterosis element has been evaluated on rhombic skew plates in bending. All generally occurring boundary and loading conditions have been included. Good agreement has been achieved between the present results and those reported in literature, even up to

reasonably large skew angles. However, obtuse corner modelling with the Heterosis element is quite poor.

REFERENCES

1. F. L. Echasz, Structural skew plates. *Trans. ASCE* 111, 1011–1042 (1946).
2. I. Mirsky, The deflection of thin flat clamped parallelogram plate subjected to uniform normal loading. Department of Supply, Australia, A. R. L., Rep. SM 175 (1951).
3. E. Reissner and M. Stein, Torsion and transverse bending of cantilever plates. *N.A.C.A., Tech. Note* 2369 (1951).
4. E. Reissner, Pure bending and twisting of skewed plates. *Q. Appl. Math* 10, 395–397 (1952).
5. F. H. Dorman, The thin clamped parallelogram plate under uniform normal pressure. Department of Supply, Australia, A.R.L., Rep. SM 214 (1953).
6. L. S. D. Morley, Bending of simply supported rhombic plate under uniform normal loading. Ministry of Aviation, London, A.R.C., 23 (1961).
7. L. S. D. Morley, Bending of simply supported rhombic plate under uniform normal loading. *Q. J. Mech. appl. Math.* XV, 413–426 (1962).
8. T. Ota and M. Hamada, Statical deflection of a rhomboidal plate with clamped edges subjected to uniformly distributed pressure. *Bull. J.S.M.E.* 6, 1–7 (1963).
9. V. Stavsky, Pure bending, twisting and stretching of skewed heterogeneous aelotropic plates. *AIAA Jnl* 1, 221–222 (1963).
10. A. Coull, The stress analysis of orthotropic skew bridge slabs. *Struct. Engr* 42, 235–241 (1964).
11. J. B. Kennedy, A fortran programme for the solution of skewed plates. *Struct Engr* 42, 49–50 (1964).
12. J. B. Kennedy and M. W. Huggins, Series solution of skewed stiffened plates. *J. Engng Mech. Div., ASCE* 90, 1–22 (1964).
13. J. B. Kennedy, On bending of clamped skewed plates under uniform pressure. *J. R. Aeronaut. Soc.* 69, 352–355 (1965).
14. A. Coull, The analysis of orthotropic skew bridge slabs. *Appl. Sci. Res.* 16, 178–190 (1966).
15. B. B. Raju and C. G. Shah, Bending of swept cantilever thin elastic plates. National Aeronautical Laboratory, Bangalore, TN-SA-7-66 (1966).
16. A. Coull, Stresses in skewed slabs. *Concrete* 1, 135–139 (1967).
17. K. T. S. R. Iyengar and R. S. Srinivasan, Clamped skew plate under uniform normal loading. *J. R. Aeronaut. Soc.* 71, 139–140 (1967).
18. A. Coull, The deformations of orthotropic skew bridge slabs. *Civ. Engng publ. Wks Rev.* 63, 55–57 (1968).
19. K. T. S. R. Iyengar and R. S. Srinivasan, Analysis of orthotropic skew bridge decks. *Bridge Struct. Engr* 1, 23–37 (1971).
20. J. B. Kennedy and D. S. R. Gupta, Bending of skew orthotropic plate structures. *J. Struct. Div., ASCE* 102, 1559–1574 (1976).
21. H. V. S. GangaRao and V. K. Chaudhary, Analysis of skew and triangular plates in bending. *Comput. Struct.* 28, 223–235 (1988).
22. L. S. D. Morley, *Skew Plates and Structures. Int. Series of Monographs on Aeronautics and Astronautics.* 5. Pergamon Press, New York (1963).
23. V. P. Jenson, Analysis of skew slabs. *Univ. of Illinois, Bull.* 39, *Engng Exp. Station Bull. Ser. No.* 332 (1941).
24. M. Naruoka and H. Ohmura, On the analysis of skew girder bridge by theory of orthotropic parallelogram plates. *Proc. IABSE* 19, 231–256 (1959).

25. K. E. Robinson, The behaviour of simply supported skew bridge slabs under concentrated load. *C.C.A., London, Res. Rep.* 8 (1959).
26. D. W. Brewster, Bending moments in elastic skew slabs. *Struct. Engr* 39, 358–363 (1961).
27. V. K. Jain, G. C. Nayak and O. P. Jain, Design of skew slab bridges for I.R.C. loadings. *J. Inst. Engrs India* 48, 1285–1296 (1968).
28. A. Razzaque, Program for triangular bending elements with derivative smoothening. *Int. J. Numer. Meth. Engng* 6, 333–343 (1973).
29. S. Timoshenko and S. Woinowsky-Krieger, *Theory of Plates and Shells*, 2nd Edn. McGraw–Hill, New York (1959).
30. J. H. Argyris, Continua and discontinua. Proc. Conf. Matrix Methods in Structural Mechanics, WPAFB, OH, pp. 112–119 (1965).
31. J. H. Argyris *et al.*, Some new elements for matrix displacement methods. Proc. Conf. Matrix Methods in Structural Mechanics, WPAFB, OH, pp. 333–398 (1965).
32. R. W. Clough and J. L. Tocher, Finite element stiffness matrices for plate bending. Proc. Conf. Matrix Methods in Structural Mechanics, WPAFB, OH, pp. 515–545 (1965).
33. D. J. Dawe, Parallelogramic elements in solution of rhombic cantilever plate problems. *J. Strain Anal.* 1, (1966).
34. H. Ramstad and I. Holand, The finite element method for the analysis of skew plates in bending using parallelogram elements. Intnl Symp. Use of Electronic Computers in Structural Engng, Univ. of Newcastle (1966).
35. P. E. West, A finite element solution to skew slab problems. *Civ. Engng publ. Wks Rev.* 61, 619–624 (1966).
36. W. C. Gustafon and R. N. Wright, Analysis of skewed composite girder bridges. *J. Struct. Div., ASCE* 94, 919–941 (1968).
37. G. R. Monforton and L. A. Schmitz, Finite element analysis of skew plates in bending. *AIAA Jnl* 6, 1150–1152 (1968).
38. W. Y. J. Shieh, S. L. Lee and R. A. Parmalee, Analysis of plate bending triangular elements. *J. Engng Mech. Div., ASCE* 94, 1089–1107 (1968).
39. F. Swako and R. J. Cope, The analysis of skew bridge decks—a new finite element approach. *Struct. Engr* 47, 215–224 (1969).
40. G. R. Monforton, Some orthotropic skew plate finite element results. *J. Struct. Div., ASCE* 98, 955–960 (1972).
41. C. K. Ramesh, V. D. Dixit and R. M. Belkune, Analysis of skew slab–beam system by finite element method. *J. Inst. Engrs India* 53, 233–239 (1973).
42. M. P. Rossow, Observations on numerical modelling of an obtuse corner of a simply supported plate. *ASME, J. appl. Mech.* 45, 689–690 (1978).
43. M. R. Vora and H. Matlock, Anisotropic skew plates and grids. *J. Engng Mech. Div., ASCE* 105, 237–253 (1979).
44. D. W. Wang, I. N. Katz and B. A. Sxabo, *h* and *p*-version of finite element analysis of a rhombic plate. *Int. J. Numer. Meth. Engng* 20, 1399–1405 (1984).
45. C. A. Felippa and P. G. Bergan, A triangular bending element based on an energy orthogonal free formulation. *Comput. Meth. appl. Mech. Engng* 61, 129–160 (1987).
46. P. G. Ming and L. F. Song, A new element used in the non-orthogonal boundary plate bending theory—an arbitrary quadrilateral element. *Int. J. Numer. Meth. Engng* 24, 1031–1042 (1987).
47. E. Reissner, The effect of transverse shear deformation on bending of elastic plates *ASME, J. appl. Mech.* 12, A69–A77 (1945).

48. R. D. Mindlin, Influence of rotatory inertia and shear deformation on flexural motions of isotropic elastic plates. *ASME, J. appl. Mech.* **18**, 31–38 (1951).

49. G. R. Monforton and M. G. Michail, Finite element analysis of skew sandwich plates. *J. Engng Mech. Div., ASCE* **98**, 763–769 (1972).

50. V. Kolar and I. Nemec, The efficient finite element analysis of rectangular and skew laminated plates. *Int. J. Numer. Meth. Engng* **7**, 309–323 (1973).

51. K. N. Ahmed and M. D. Mathers, Finite element analysis of anisotropic plates. *Int. J. Numer. Meth. Engng* **11**, 289–307 (1977).

52. T. J. R. Hughes, M. Cohen and M. Haroun, Reduced and selective integration techniques in finite element analysis of plates. *Nucl. Engng Des.* **46**, 203–222 (1978).

53. V. A. Pulmano and P. K. Lim, Elastic analysis of skew thick plates by finite prism method. Intnl Conf. on Comput. Applic. in Civil Engng, Roorkee, India, pp. 121–126 (1979).

54. T. J. R. Hughes and T. E. Tezduyar, Finite elements based upon Mindlin plate theory with particular reference to the four-noded bilinear isoparametric element. *ASME, J. appl. Mech.* **48**, 587–596 (1981).

55. T. Belytschko and C. S. Tsay, A stabilization procedure for the quadrilateral plate element with one point quadrature. *Int. J. Numer. Meth. Engng* **19**, 405–419 (1983).

56. D. R. J. Owen and J. A. Figueiras, Anisotropic elastoplastic finite element analysis of thick and thin plates and shells. *Int. J. Numer. Meth. Engng* **19**, 541–566 (1983).

57. T. Beltyschko, J. S. J. Ong and W. K. Liu, A consistent control of spurious singular modes in the 9 node-Lagrangian element for the Laplace and Mindlin plate equations. *Comput. Meth. appl. Mech. Engng* **44**, 269–295 (1984).

58. J. C. Boot and D. B. Moore, An efficient analysis for thin plates of general quadrilateral shape subjected to bending stresses. *Comput. Meth. appl. Mech. Engng* **43**, 57–79 (1984).

59. M. A. Crisfield, A quadratic Mindlin element using shear constraints. *Comput. Struct.* **18**, 833–852 (1984).

60. A. Tessler and T. J. R. Hughes, A three node Mindlin plate element with improved transverse shear. *Comput. Meth. appl. Mech. Engng* **50**, 71–101 (1985).

61. E. Hinton and H. C. Huang, A family of quadrilateral Mindlin plate elements with substitute shear strain fields. *Comput. Struct.* **23**, 409–431 (1986).

62. A. F. Saleeb and T. Y. Chang, An efficient quadrilateral element for plate bending analysis. *Int. J. Numer. Meth. Engng* **24**, 1123–1155 (1987).

63. O. C. Zienkiewicz and D. Lefebvre, A robust triangular plate bending element of the Reissner–Mindlin type. *Int. J. Numer. Meth. Engng* **26**, 1169–1184 (1988).

64. G. Prathap and B. R. Somashekar, Field and edge consistency synthesis of a 4-noded quadrilateral plate bending element. *Int. J. Numer. Meth. Engng* **26**, 1693–1708 (1988).

65. D. Briassoulis, Machine locking of degenerated thin shell elements. *Int. J. Numer. Meth. Engng* **26**, 1749–1768 (1988).

66. H. U. Akay, An investigation of first and second order mixed plate bending elements. *Int. J. Numer. Meth. Engng* **15**, 351–360 (1980).

67. J. L. Batoz, A study of three node triangular plate bending elements. *Int. J. Numer. Meth. Engng* **15**, 1771–1812 (1980).

68. J. Jirousek and N. Leon, A powerful finite element for plate bending. *Comput. Meth. appl. Mech. Engng* **12**, 77–96 (1977).

69. J. Jirousek, Hybrid–Trefftz plate bending elements with p-method capabilities. *Int. J. Numer. Meth. Engng* **24**, 1367–1393 (1987).

70. M. A. Crisfield, A four-noded thin plate bending element using shear constraints—a modified version of Lyons' element. *Comput. Meth. appl. Mech. Engng* **38**, 93–120 (1983).

71. L. S. D. Morley, Bending of clamped rectilinear plates. R.A.E. report on Structures, Z89 (1963).

72. L. S. D. Morley, Bending of clamped rectilinear plates, *Q. J. Mech. appl. Math.* **27**, 293–317 (1964).

73. J. B. Kennedy, Clamped skew plate under uniform normal loading. *Aeronaut. J. R. Aeronaut. Soc.* **72**, 338–340 (1968).

74. H. A. Hadid, B. M. Ahuja and B. M. Ali, Static analysis of clamped skew plates. *Bridge Struct. Engr* **9**, 39–64 (1979).

75. K. R. Ruston, Electrical analogue solutions for deformation of skew plates. *Aeronaut. Q.* **XV**, 169–180 (1964).

76. C. T. Harden and K. R. Ruston, The analysis of four span skew bridge using an electrical analogue computer. *Proc. Instn Civ. Engrs* **36**, 297–324 (1967).

77. W. E. Warren, Bending of rhombic plates. *AIAA Jnl* **2**, 166–168 (1964).

78. S. S. Sattinger and H. D. Conway, Solution of certain isosceles triangle and rhombus torsion and plate problems. *Int. J. Mech. Sci.* **7**, 221–228 (1965).

79. B. D. Aggarwal, Bending of rhombic plates. *Q. J. Mech. appl. Math.* **19**, 79–82 (1966).

80. B. D. Aggarwal, Bending of parallelogram plates. *J. Engng Mech. Div., ASCE* **93**, 4, 9–18 (1967).

81. A. L. Yettram, An equivalent grid framework for skew plates in flexure. *Int. J. Mech. Sci.* **14**, 407–416 (1972).

82. T. G. Brown and A. Ghali, Semi-analytical solution of skew plates in bending. *Proc. Instn Civ. Engrs* **57**, 165–174 (1974).

83. T. G. Brown and A. Ghali, Semi-analytical solution of skew box girder bridges. *Proc. Instn Civ. Engrs* **59**, 487–500 (1975).

84. M. Mukhopadhyay, Finite strip method of analysis of clamped skew plates in bending. *Proc. Instn Civ. Engrs* **61**, 189–195 (1976).

85. Y. K. Cheung and Z. Dashan, Large deflection analysis of arbitrary shaped thin plates. *Comput. Struct.* **26**, 811–814 (1987).

86. J. B. Kennedy and I. C. Martens, Stresses near corners of skew stiffened plates. *Struct. Engr* **41**, 345–346 (1963).

87. A. Coull and G. Lickiss, Continuous skew slabs by Moire Fringe method. *Civ. Engng publ. Wks Rev.* **60**, 215–217 (1965).

88. R. M. Tiller, Analysis of skew slabs by use of influence surfaces. *Civ. Engng publ. Wks Rev.* **63**, 415–419 (1968).

89. M. J. Marchant and M. B. Snell, Determination of flexural stiffness of thin plates from small deflection measurements using Optical Holography. *J. Strain Anal.* **17**, 53–61 (1982).

90. J. B. Kennedy and N. G. Simon, Linear and non-linear analysis of skewed plates. *ASME, J. appl. Mech.* **34**, 271–277 (1967).

91. R. S. Alwar and N. R. Rao, Large elastic deformations of clamped skew plates by dynamic relaxation. *Comput. Struct.* **4**, 381–393 (1974).

92. R. S. Srinivasan and S. V. Ramachandran, Large deflection of clamped skew plates. *Comput. Meth. appl. Mech. Engng* **7**, 219–233 (1976).

93. T. J. R. Hughes and M. Cohen, The "Heterosis" finite element for plate bending. *Comput. Struct.* **9**, 445–450 (1978).

94. E. Hinton and D. R. J. Owen, *Finite Element Software for Plates and Shells*. Pineridge Press, Swansea, U.K. (1984).

95. M. P. Rossow, Efficient C^0 finite element solution of simply supported plates of polygonal shape. *ASME, J. appl. Mech.* **44**, 347–349 (1977).